The Effects of Soil Surface Temperature and Relative Humidity on 2, 4-D Volatilization

by

Pan Wang

A thesis submitted to the Graduate Faculty of
Auburn University
in partial fulfillment of the
requirements for the Degree of
Master of Science

Auburn, Alabama
May 6, 2018

Keywords: 2,4-D, Volatilization, Monolayer water, Isotherm, Specific Surface Area

Approved by

Thorsten Knappenberger, Assistant Professor of Crop, Soil and Environmental Sciences
Joey N. Shaw, Professor of Crop, Soil and Environmental Sciences
Yucheng Feng, Professor of Crop, Soil and Environmental Sciences
Steve Li, Extension Specialist and Assistant Professor of Crop, Soil and Environmental Sciences

Abstract

Monolayer water content and specific surface area are two of the most significant characteristics of soil. The monolayer water content (m_0) and specific surface area measurements were made by both Brunauer Emmett Teller (BET) and Guggenheim, Anderson and De Boer (GAB) method of adsorption of water molecules. Two replicate measurements of monolayer water content and specific surface area were performed for nine source clay minerals from The Clay Minerals Society and three benchmark soils from Alabama. Overall, the commonly used BET equation gives the lower monolayer water content and specific surface area values compared with GAB.

The water vapor sorption isotherm (WSI) of a soil describes the relationship between the relative humidity and water content. The WSIs in this study were developed by Vapor Sorption Analyzer (VSA) with relatively high resolution and a reasonable time compared with the traditional method. Overall the sorption isotherms show the positive relationship between relative humidity and soil water content, in which the relative humidity ranges from 0.03 to 0.95. The adsorption isotherm has a lower water content than the desorption isotherm at a given relative humidity. The hysteresis phenomenon between the absorption and desorption isotherm is evident for all test media.

2,4-Dichlorophenoxyacetic acid (2,4-D) is one of the first commercially available herbicide since 1940s and it is a relatively large group of herbicides that had a revolutionary effect on agriculture. 2,4-D volatilization experiments in a lab scale were conducted for four clay minerals and three benchmark soils with four different relative humidity (RH) levels for $24\,\mathrm{h}$, two lower than the m_0 corresponding RH and two higher. The RH regimes were given by the VSA. Results show the volatilization rate of 2,4-D was relatively high for each test media and each RH level (range from 50-80$\%$), the influence of RH on 2,4-D volatilization is significant (P=0.04), and the

volatilization rate of 2,4-D differs among test media, the volatilization is lower when RH lower than m_0 corresponding RH (P=0.01).

Acknowledgments

I would first like to thank my major advisor Dr. Thorsten Knappenberger, the door to Dr. Knappenberger′office was always open whenever I ran into a trouble spot or had a question about my research or writing. His guidance helped me all the time of research and writing of this thesis. I′m so grateful for the support and help for the last couple years.

Besides my advisor, I would also spread my thankful to Joey Shaw, Yucheng Feng and Steve Li for serving as my committees. Thank you so much for your help, encouragement, insightful comments, which greatly improved our research.

I would also thanks for Jianping Wang with the assistance of HPLC, her advices and comments greatly improved my research, she spent so much time working on establishing analysis method for me. I also thanks Dr. Arthur from Aarhus University, Denmark for providing me with the GAB model which made my research more smoothly.

Finally, I must express my very profound gratitude to my parents: Yinliang Wang and Shuang Cheng for providing me with unfailing support and continuous encouragement throughout my years of study and through the process of researching and writing this thesis. This accomplishment would not have been possible without them.

Table of Contents

List of Figures

List of Tables

List of Abbreviations

ABL	Atmospheric Boundary Layer
ACN	Acetonitrile
BDDT	Brunauer, Deming, Deming, and Teller
BET	Brunauer Emmett Teller
CEC	Cation Exchange Capacity
DDI	Dynamic Dew point Isotherm
DVS	Dynamic Vapor Sorption
GAB	Guggenheim, Anderson and De Boer
GE	Genetically Engineered
HPLC	High Performance Liquid Chromatography
HR	Herbicide Resistant
IUPAC	International Union of Pure and Applied Chemistry
Ksat	Saturated Hydraulic Conductivity
m_0	Monolayer Water Content
ML	Monolayer Water Content
PRM	Revolutions Per Minute
RH	Relative Humidity

SI Step Isotherm

SSA Specific Surface Area

SWCC Soil Water Characteristic Curve

UPLC Ultra Performance Liquid Chromatography

USDA The US Department of Agriculture

WSI Water vapor Sorption Isotherm

Chapter 1

Literature Review

1.1 Clay Minerals and Benchmark Soils

Clay minerals are the characteristic minerals of the earth near surface environments. They form in soils and sediments and by diagenetic and hydrothermal alteration of rocks. Clays are silicates that belong to the phyllosilicate group. Water is essential for clay mineral formation, and most clay minerals are described as hydrous aluminosilicates. Structurally, the clay minerals are composed of planes of cations, arranged in sheets, which may be tetrahedrally or octahedrally coordinated, which in turn are arranged into layers often described as 2:1 if they involve units composed of two tetrahedral and one octahedral sheet or 1:1 if they involve units of alternating tetrahedral and octahedral sheets. Additionally, some 2:1 clay minerals have interlayer sites between successive 2:1 units which may be occupied by interlayer cations, which are often hydrated (Middleton, 2003). The classification of the phyllosilicate clay minerals is based on the features of layer type (1:1 or 2:1), the dioctahedral or trioctahedral character of the octahedral sheets, the magnitude of any net negative layer charge due to atomic substitutions, and the nature of the interlayer material (Hillier, 2017).

1.1.1 Clay Minerals

Kaolinite is one of the most common clay minerals, the chemical composition is $\mathrm{Al_2Si_2O_5(OH)_4}$. It is a layered silicate mineral, with one tetrahedral sheet of silica ($\mathrm{SiO_4}$) linked through oxygen atoms to one octahedral sheet of alumina ($\mathrm{AlO_6}$) octahedral (Deer, 2013), which also be called 1:1 layer type clay. Kaolinite has a low shrink-swell capacity and a low cation-exchange capacity ($0.01\,\mathrm{mol\,kg^{-1}}$ to $0.15\,\mathrm{mol\,kg^{-1}}$). It is a soft, earthy, usually white,

mineral (dioctahedral phyllosilicate clay), produced by the chemical weathering of aluminum silicate minerals like feldspar (Data, 2001).

Smectite is the name used for a group of phyllosilicate mineral species, the most important of which are montmorillonite, beidellite, nontronite, saponite and hectorite (Odom, 1984). There and several other less common species are differentiated by variations in chemical composition involving substitutions of Al for Si in tetrahedral cation sites and Al, Fe, Mg and Li in octahedral cation sites. Smectite clays have a variable net negative charge, which is balanced by Na, Ca, Mg and, or, H adsorbed externally on interlamellar surfaces. Smectite is 2:1 layer type clay (Hillier, 2017), the structure, chemical composition, exchangeable ion type and small crystal size of smectite clays are responsible for several unique properties, including a large chemically active surface area, a high cation exchange capacity, interlamellar surfaces having unusual hydration characteristics, and sometimes the ability to modify strongly the flow behavior of liquids.

1.1.2 Benchmark Soils

A benchmark soil is one of large extent within one or more major land resource areas (MLRA), which holds a key position in the soil taxonomic system. Generally there is a large amount of data, and it has special importance to significant land uses, or it is important for ecology (Hammer, 2017). The complete data set of a benchmark soil contains clay, organic carbon, extractable Na, $\mathrm{NH_4OAC}$ based CEC, pH, mineralogy, infiltration, bulk density, Ksat, seasonal water table location, depth, etc. With the benchmarks soil data set, it is possible to acquire significant information for a soil of regional importance, and extrapolate that information to related or neighboring soils. Knowledge of the properties and behavior of benchmark soils contributes to the understanding and interpretation of other soils with similar properties.

Benchmark soils can be selected for their representativeness and included in studies of single soil or a suite of soils, such as those representing a gradient in temperature or moisture across a region. The list and accompanying information about the soil's classification, land uses, land cover, and ecological significance are useful in the development of cross-site studies or networks

(NRSC, 2016). Some example uses for benchmark soils are: extending estimated soil property data to similar soil, documenting soil properties for ecological site descriptions, assessing conservation effects, evaluating soil interpretations, studying macro/micronutrient and trace elements, monitoring change in soil quality and natural resource condition, measuring saturated hydraulic conductivity, documenting attainable dynamic soil property values for specific management systems, etc.

In this study, soils from the Orangeburg, Dothan and Cecil series were used because they are common and representative benchmark soils in Alabama. The Orangeburg series (Figure1.1a) consists of very deep, well drained, moderately permeable soils on uplands of the Southern Coastal Plain. They formed in loamy and clayey marine sediments. The average annual temperature is about $18\,^{\circ}\mathrm{C}$, and the average annual precipitation is about $132\,\mathrm{cm}$. Slopes range from $0\,\%$ to $25\,\%$. The series is of large extent, it distributes southern coastal plain of Alabama, Arkansas, Florida, Georgia, Louisiana, North Carolina, South Carolina and Virginia (NRCS, 2014). The taxonomic class of Orangeburg series soil is Fine-loamy, kaolinitic, thermic Typic Kandiudults.

The Dothan series (Figure1.1b) consists of very deep, well drained soils that formed in thick beds of unconsolidated, medium to fine-textured marine sediments. Dothan soils can be found on interfluves which is an area of higher ground between two rivers in the same drainage system, and the slopes range from $0\,\%$ to $15\,\%$. Mean annual temperature is about $18\,^{\circ}\mathrm{C}$ and the mean annual precipitation is about $136\,\mathrm{cm}$. The series occurs primarily in the southern coastal plain, but it also occurs to a lesser extent in the Atlantic Coast Flatwoods (NRCS, 2017b). The taxonomic class of Dothan series soil is Fine-loamy, kaolinitic, thermic Plinthic Kandiudults.

The Cecil series (Figure1.1c) consists of very deep, well drained moderately permeable soils on ridges and side slopes of the Piedmont uplands. They are deep to saprolite and very deep to bedrock. They formed in residuum weathered from felsic, igneous and high-grade metamorphic rocks of the Piedmont uplands. Slopes range from $0\,\%$ to $25\,\%$. Mean annual precipitation is $122\,\mathrm{cm}$ and mean annual temperature is $15\,^{\circ}\mathrm{C}$. The series is of large extent, with an area of more than 4 million hectares, which distributes the Piedmont of Alabama, Georgia, North Carolina,

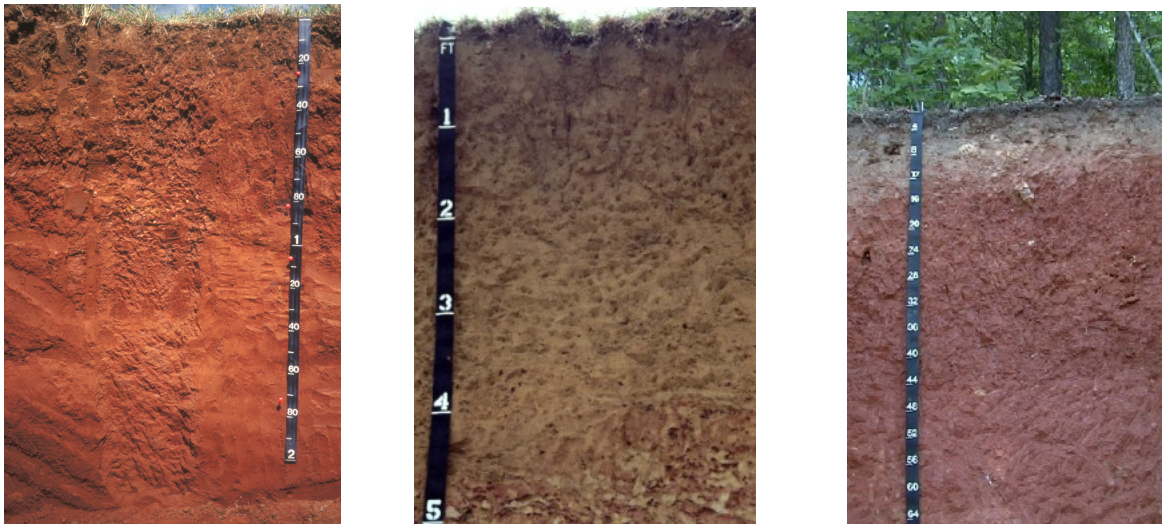

(a) A Profile of Orangeburg Soil. (b) A Profile of Dothan Soil. (c) A Profile of Cecil Soil.

Figure 1.1: Profiles of the Benchmark Soils from Alabama (NRCS, 2017d,c,a).

South Carolina, and Virginia (NRCS, 2007). The taxonomic class of Cecil series soil is Fine, kaolinitic, thermic Typic Kanhapludults.

1.2 Water Vapor and Soil Mineral Interaction

The process of adsorption and desorption of water vapor to the soil mineral surface is called soil mineral hydration. The process of soil mineral hydration can be described by the water vapor sorption isotherm.

1.2.1 Water Sorption Isotherm

The water vapor sorption isotherm (WSI) of a soil describes the relationship between relative vapor pressure (water activity, a_w) and water content (Callum Hill, 2009), in which water activity is defined as the ratio of partial pressure of water vapor in the soil (P) to that in presence of pure water (P_0) (Mathlouthi, 2001). It represents the variation of water content as a function of water activity at a given, constant temperature along an adsorption or desorption path, adsorption for increasing humidity and desorption for decreasing humidity. Sorption of water vapor by soil shows a hysteresis phenomenon (Figure 1.2), adsorption and desorption curves are not

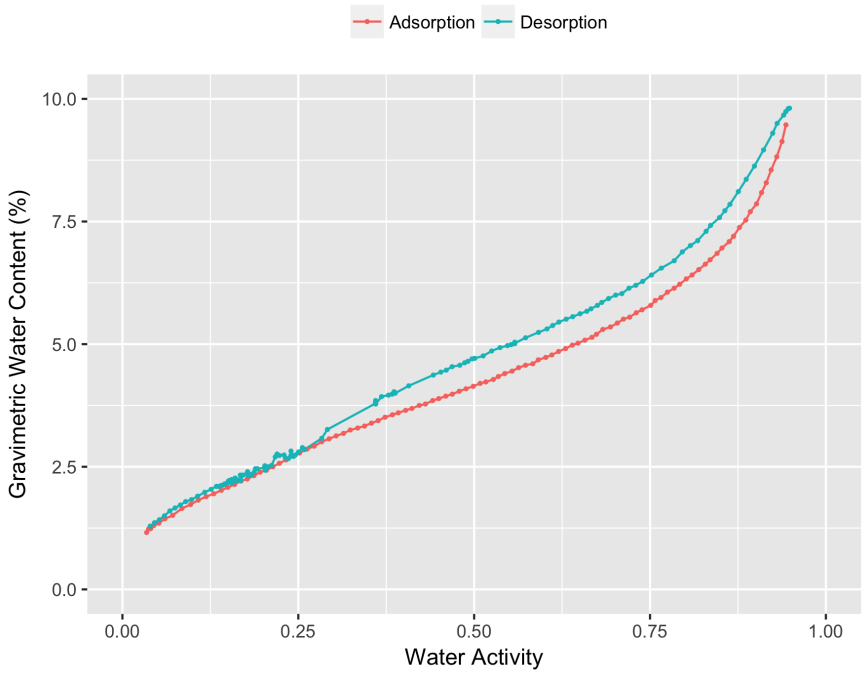

Figure 1.2: Water Vapor Sorption Isotherm of Illite-Smectite.

superposed, this phenomenon is evident for all soils. When the soil wets from air dryness or dries from saturation, the characteristics are called primary wetting or drying curves. The wetting curve always has a lower water content for a given potential than does the drying curve. Mechanisms for it including particle surface hydration and interlayer cation hydration are discussed by Lu and Khorshidi (2015), the reason for the hysteretic behavior of the water retention curve is the formation of bottlenecks and empty pores in the soil pore network (in particular during wetting), which often determine partial saturation of soil pores and therefore results in a curve with a different shape from the drying curve. Knowledge of the water sorption isotherm is essential for various tasks like predicting the sorption of organic vapors to mineral surfaces or for a better understanding of the water balance in dry soils (Schneider and Goss, 2012).

The first systematic attempt to interpret adsorption isotherms for gas-solid was introduced by Brunauer, Deming, Deming, and Teller (BDDT) in 1940 (Brunauer et al., 1940). These authors classified isotherms into five types. The BDDT classification has become the core of the modern IUPAC classification of adsorption isotherms (Rouquerol et al., 1994). The BDDT isotherms and

an additional one introduced much later by Sing, which completes the IUPAC classification, are illustrated in Figure 1.3. All sorption isotherms should at least fit one, or a combination of two or more, of the six types of isotherms.

The general shape of a sorption isotherm is sigmoidal, which indicate to a Type II isotherm according to the classification of IUPAC system. This type of isotherm can be divided into three stages (Industrial and Pino, 2005). Zone 1 of the sorption isotherm shown in Figure 1.4 is the result of Van der Waals forces on water molecules. The water molecules sorb onto the available sorption sites rapidly until a monolayer is formed, which covers the external surface of the soil particle. At this moment, water exists as a rigid state due to the chemical bonds. The next zone is produced when this first layer is saturated. It is characterized by the adsorption of water molecules on the first layer resulting in the creation of more water molecule layers. The isotherm in this zone can be represented graphically as growing linearly. In zone 3, it is possible to find water in the liquid state in the soil capillaries. If we assume that in the interface from zone 2 to zone 3 the adsorbed water covers the soil particles homogeneously, the water molecule layer is thick enough to form liquid water in the pores between soil particles by capillary condensation. Thus, micro capillary water starts to form a continuous phase.

In the past, the WSI was accomplished by dynamic vapor sorption method (Goss and Madliger, 2007), which is by exposing a soil sample to a series of step changes in relative humidity and monitoring the mass change as a function of time. The sample mass must be allowed to reach gravimetric equilibrium at each step change in humidity before progressing to the next humidity level. Then, the equilibrium mass values at each relative humidity step are used to generate the isotherm. However, this method is very time-consuming. The recent WSI measurement technology is advanced, the WSI of a soil can be developed by Vapor Sorption Analyzer (Meter Environment, Pullman WA) (Figure 1.5) with relatively high resolution and a reasonable time, usually 1-3 days, even for high fine-textured soil (Arthur et al., 2016), while the traditional method takes several weeks for one soil sample.

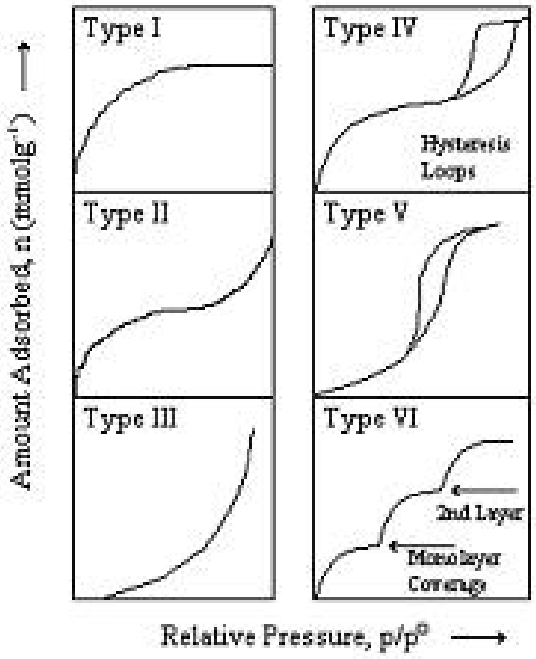

Figure 1.3: Diagrammatic Representation of Isotherm Classification (Brunauer et al., 1940).

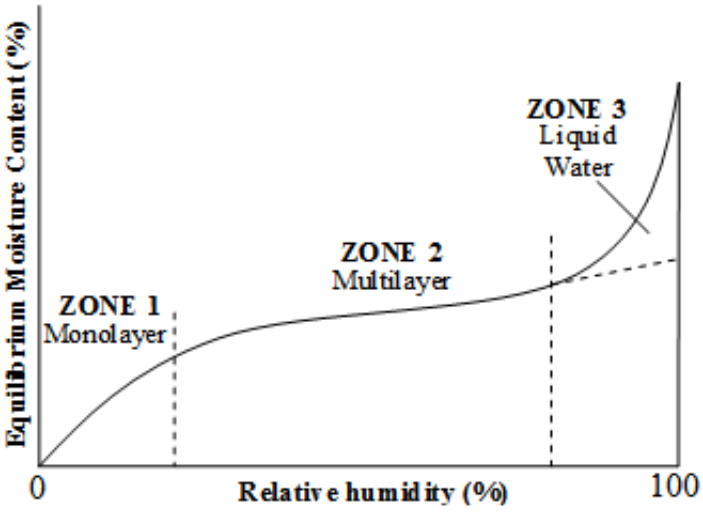

Figure 1.4: General Shape of Sorption Isotherms.

Figure 1.5: Vapor Sorption Analyzer (Meter Environment, 2017).

1.2.2 BET and GAB Theories

Several mathematical functions that describe WSIs for various materials have been proposed in literatures. BET and GAB models are two of them which are relatively common (Dogan et al., 2006; Fujita, 1963; Maroulis et al., 1988; Prothon and Ahrne, 2004). The BET model is firstly reported in 1938 (Brunauer et al., 1938), it is based on theory of statistical thermodynamics. BET model is widely used in the food industry (Maroulis et al., 1988; Kiranoudis et al., 1992; Mali et al., 2005) and it is based on the application of the Langmuir equation to the first and subsequent layers of adsorbate on the surface. In the BET model, the heat of adsorption of the second and following monolayers is assumed to be constant and equal to the heat of liquefaction. Two basic assumptions for the derivation of the BET equation are: (1) the surface of the adsorbent is homogeneous, and (2) there is no lateral interaction between the adsorbed molecules. The Specific Surface Area (SSA) of a soil can be estimated by the BET model. The monolayer water content (m_0) of a soil is the water content when the soil particle is covered by only a monomolecular layer, the m_0 can also be estimated by BET. The BET isotherm is expressed by the following equation:

$$\frac{a_w}{(1-a_w)m} = \left[\frac{c-1}{m_0 c}\right] a_w + \frac{1}{m_0 c} \tag{1.1}$$

where a_w is the water activity, m is the water content (dry basis), m_0 is the monolayer water content and c is dimensionless constant that is related to the enthalpy of adsorption of the adsorbate gas on the powder sample. This relation is applicable for $a_w < 0.55$.

There are three regions in the water vapor sorption isotherm: A, B and C (Figure 1.6a). Region A is corresponding to hydration monolayer where water molecules are bonded to the soil by strong H-bond. Region B corresponds to the linear part of the sorption isotherm. Water is adsorbed as multilayers of molecules of hydrogen bonded to the monolayer, or entrapped in the soil by capillarity, Van der Waals forces, etc. Region C is that of the so-called "free" or solvent water. Water molecules in this region are much less strongly bound than in regions A and B. This fraction of water is available for mould growth or dissolving of soluble solutes.

The monolayer water content m_0 can be determined graphically (Figure 1.6b). In this graph, the x axis is water activity, y axis is a term that related to water content and water activity. According to the BET equation, the slope of the linear model can be expressed by $\frac{c-1}{m_0 c}$ and the intercept is $\frac{1}{m_0 c}$, the m_0 can be calculated by

$$m_0 = 1/(intercept + slope) \tag{1.2}$$

The GAB model is a modified version of the BET model. Other than the BET model, the GAB model postulates that the heat of adsorption of the second and following monolayers is constant, but less than the heat of liquefaction (Louis B. Rockland, 1981), and the GAB model has one more parameter than BET. The GAB model is also a statistical thermodynamics basis theory. In general, the GAB equation is considered the most versatile due to its ability to cover a wider a_w range. It has been recommended by the European Project Group COST 90 for physical properties of food (Wolf et al., 1984). The GAB model can be expressed by the following equation:

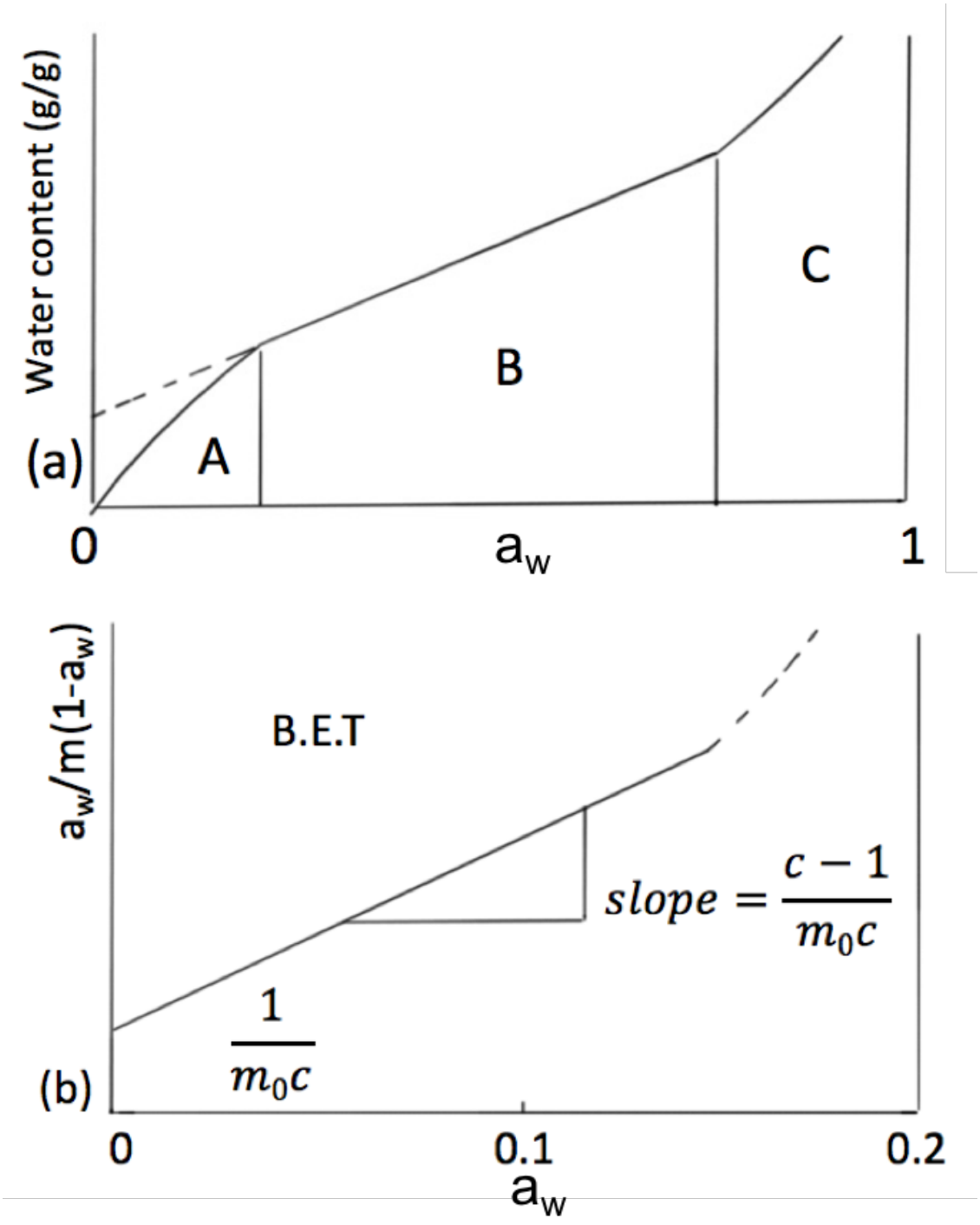

Figure 1.6: **(a)** Three regions of water vapor sorption curve, **(b)** Determination of monolayer water content by using the BET model.

$$\frac{a_w}{m} = \frac{mcka_w}{(1 - ka_w)(1 + (c-1)ka_w)} \tag{1.3}$$

where a_w is the water activity; m is the water content (dry basis); m_0 is the monolayer water content, c and k are energy constants.

Timmermann et al. (2001) conducted an experiment on the two models, the object of this study was to determine the difference between the values of the monolayer and the energy parameters obtained by the regression of water sorption data by using BET two-parameter isotherm or the GAB three-parameter isotherm. The results showed that the GAB values are more general and have more physical meaning.

The specific surface area is one of the most significant characteristics of soil and sediments (Catherine N. Mulligan, 2009), and it is well known that the SSA of soil is influenced by the mineral type and content (Bingham et al., 1978), organic matter content (Feller, 1992), the degree of inter-particle association (Schulze and Schwertmann, 1984), and also the average size of the particles (Schwertmann, 1985). Since m_0 is directly related to the SSA (Akin and Likos, 2014), it is also influenced by these factors. The SSA can be calculated by the following equation:

$$SSA = \frac{m_0}{m_w} \times N \times A \tag{1.4}$$

In which m_W is the molecular mass of water (0.018 kg mol^{-1}), N is the Avogadro$'$s number (6.023×10^{23} mol^{-1}), A is the area covered by one H_2O molecule (A= $10.8 \times 10^{-8} m^2$).

1.3 Monolayer Water Content

Water confined on the nanometer scale usually exhibits behavior different from bulk systems and significantly depends on the structure of nanoscale systems (Wang et al., 2011). Soil monolayer water content (m_0) is the soil water content when the soil particle is covered by one layer of water molecules (Figure 1.7). When m is below m_0, the soil is covered by water partly, and part of the soil exposes to the atmosphere directly (Figure 3a). Since the soil is negative

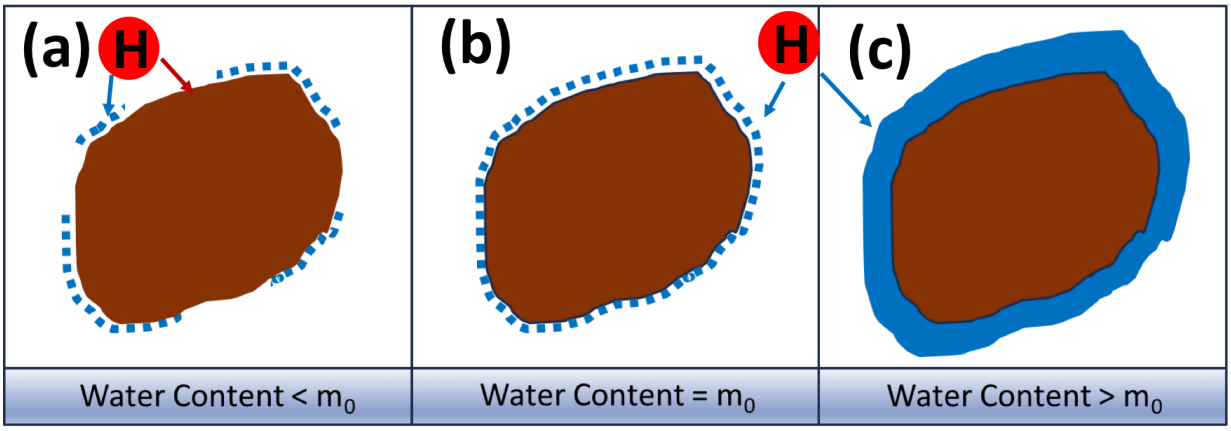

Figure 1.7: **(a)** Soil particle is covered by water molecules partly when soil water content (m) is lower than monolayer water content (m_0), herbicide can be absorbed either by soil mineral surface or water molecule film. **(b)** Soil particle is covered by one layer of water molecules. **(c)** Soil particle is covered by multiple layers of water molecules. Herbicide can be absorbed only by water film when m is equal or higher than m_0.

charge, the soil has stronger ability to absorb most ionizable herbicide than water. In situations where the soil water content is at or above the monolayer water content (Figure 3b+c) we expect more volatilization due to the lack of adsorption sites on the soil mineral surface.

1.4 Volatilization

Volatilization is the process that a dissolved sample is vaporized. Herbicide volatilization refers to evaporation or sublimation of a volatile herbicide, and it is a significant loss pathway that may have unintended consequences in non-target environments (Prueger et al., 2005). It has been recognized that highly volatile pesticides were lost from plant or soil surfaces mainly by vaporization into the atmosphere, and pesticides range in volatility from fumigants, such as gaseous methyl bromide, to herbicides with vapor pressures below 1.3×10^{-9} Pa (Spencer et al., 1973). 2,4-D and dicamba are commonly used herbicides that are known to be subject to volatilization (Pollack, 2012). The effect of gaseous herbicides is lost at its intended place of application and move downwind and affect other plants not intended to be affected causing crop damage.

The loss of herbicide by volatilization is greater than runoff. Runoff losses of pesticide are typically less than $1\,\%$ of the amount that applied, although levels can be exceeded when precipitation occurs immediately after application (Wauchope, 1978; Gaynor et al., 2002), while volatilization losses can range from $5\,\%$ to $90\,\%$ of the amount applied, depending on the pesticide properties, management practices, soil properties, mode of application, and regional and local meteorological conditions (Taylor and Spencer, 1990; Prueger et al., 1999; Gish et al., 2009). An eight years study was conducted by Gish et al. (2011) to better understand factors influencing year to year variability in field scale herbicide volatilization and surface runoff losses, the results showed herbicide volatilization is much greater than runoff losses ($P < 0.007$) (Gish, 2017) and when averaged over two herbicides evaluated (Metolachlor and Atrazine), loss by volatilization was more than 25 times larger than surface runoff losses.

Daytime herbicide (metalochlor) volatilization losses were significantly greater than nighttime vapor losses ($P < 0.05$), volatilization occurred diurnally and accounted for between $43\,\%$ to $86\,\%$ during the day and $14\,\%$ to $57\,\%$ during the night of the total measured loss (Prueger et al., 2005).

Most of the herbicide volatilization happened in the first $72\,\mathrm{h}$ after application. Prueger et al. (2005) conducted a study about factors effects on metolachlor, the cumulative volatilization losses for the 120-hour period following metolachlor application varied over the years from $5\,\%$ to $25\,\%$ of the applied active ingredient, with approximately $87\,\%$ of the losses occurring during the first $72\,\mathrm{h}$.

Prueger et al. (2005) studied on the solar radiation, relative humidity, and soil water effects on metolachlor volatilization, results showed differences in meteorological conditions and surface soil water contents resulted in the variability of the volatilization losses. The peak volatilization losses for each year occurred during the first $24\,\mathrm{h}$ after application with a maximum flux rate associated with wet surface soil conditions combined with warm temperatures.

Martina Schneider and Goss (2013) studied the volatilization of pesticides from soils under dry conditions which were trifluralin and triallate. Results showed the volatilization rate of pesticides could be significantly influenced by sorption to the hydrated mineral surface. This

experiment started with very dry conditions, the volatilization rate of pesticides increases up to 8 times with an increasing RH from $60\,\%$ to $85\,\%$. There was an additional strong increase of volatilization rate caused by a simulated rain event (0.5-0.7mm), which due to the elimination of all sorption sites associated to soil mineral surface. This study suggested that the surface area of mineral was the soil property that governs the volatilization of pesticides under dry conditions, and soil organic matter content was the controlling variable under wet conditions. This study demonstrated that relative humidity effects on pesticide volatilization could be interpreted via the mechanism of sorption to the mineral surface under dry conditions.

1.5 Properties and Application of 2,4-Dichlorophenoxyacetic Acid

2,4-Dichlorophenoxyacetic acid, commonly known as 2,4-D, was one of the first commercially available herbicides. 2,4-D is one of the oldest herbicides used in the United States. Today, 2,4-D continues to be one of the most commonly used herbicides on the market (Tu et al., 2001).

It is the most commonly used herbicide in the non-agricultural industry and also one of the most commonly used herbicides in the agricultural industry, it was being used for 25-29 million kg annually in the U.S. (Grube and Donaldson, 2011). 2,4-D is a general use herbicide, which means it can be used on a variety of food sites including field, fruit, and vegetable crops. 2,4-D is a post-emergence control herbicide that used to kill broadleaf weeds.

1.5.1 Properties of 2,4-D

2,4-D is produced in several forms, including acids, salts, amines and esters, and the toxicity is varying among different forms. The currently registered forms of 2,4-D are 2,4-D acid, 2,4-D sodium salt, 2,4-D diethylamine, 2,4-D dimethylamine salt, 2,4-D isopropyl acid, 2,4-D triisopropyl acid, 2,4-D butoxyethyl ester, 2,4-D ethylhexyl ester and 2,4-D isopropyl ester (Anon, 2015). Approximately $90\,\%$ to $95\,\%$of the global use was taken by the dimethylamine salt

(DMA) and ethylhexyl ester (EHE) forms (Charles JM, 2001). The ester form of 2,4-D is considered the most volatile and can be stayed in the air for longer periods of time (University, 2017). The most volatile of the 2,4-D esters are methyl and isopropyl, which have been banned in the U.S. (Que Hee and Sutherland, 1974), but there still are some volatile ester formulations of 2,4-D remain available in the market. The degree of volatile is inversely related to the length of the ester chain. Today only 2,4-D amine and low volatile ester 2,4-Ds are sold. 2 4-D choline, which is newly registered in December 2014, is less prone to drift and volatilization than other formulations (EPA, 2015).

Weed science has already determined that there is no significant difference in the performance of 2,4-D low volatile ester and 2,4-D amine. 2,4-D amine is nearly nonvolatile and can be used during spring or summer periods, low volatile 2,4-D products can be used during fall cooler periods (when daytime highs are less than $10\,^{\circ}\mathrm{C}$) assuming there are no adjacent broadleaf plants or trees at risk if temperatures happen to rise (Delvalle, 2017).

2,4-D belongs to phenoxy carboxyl acid herbicide, and this is a relatively large group of herbicides that had important effect on agriculture. They are all growth regulators in that they have a hormone-like activity. This is reflected in their excellent translocation properties and their effectiveness at low rates. While 2,4-D is normally applied to plant's leaves, it can be absorbed by the roots and stems, 2,4-D remains at high levels within plant tissues and causes rapid cell growth. Plants die when their vascular transport systems become blocked and destroyed by abnormally fast growth. So 2,4-D is much more toxic to vascular plants than to non-vascular plants (Anon, 2015).

Rochette (1996) studied the interaction of soil components with 2,4-D acid under supercritical fluid conditions. Three potential factors inhibiting 2,4-D extraction from soil were selected for the test, which were (1) adsorption to mineral surfaces, (2) diffusion-limited release from porous materials, and (3) pH-dependent partitioning between the solid and supercritical fluid phases. Results showed soil pH was the main chemical factor that affecting 2,4-D recovery. Rochette (1996) contend organic matter will generally be the main component limiting extraction of 2,4-D from soils due to its porosity, pH buffering capacity, and ubiquitous occurrence.

Furthermore, methanol enhances 2,4-D recovery, because the protonated form of 2,4-D is favored due to the higher pKa of 2,4-D in this solvent compared to water, because the ionized form will not dissolve in a nonpolar fluid unless an ion pair is formed.

1.5.2 2,4-D Application Concerns

Herbicide spray drift is the movement of herbicide from the target area to areas where herbicide application was not intended. Herbicide drift generally is caused by movement of spray droplets or herbicide vapors (Dexter, 1995). It can occur with any herbicides, and the risk of damage to non-target plants varies considerably among herbicides as well as non-target plants.

Dow AgroSciences carried out a recent survey on the percent of crop hectares in the U.S. impacted by glyphosate-resistant weeds. Findings from the survey were provided to the USDA in support of Dow AgroSciences's petition for deregulation of 2,4-D herbicide-resistant corn, and the findings suggest that around $4 \times 10^7\,\mathrm{kg}$ are already impacted by glyphosate-resistant weeds. The true extent of spread in the U.S. likely lies around the midpoint between the WSSA and Dow AgroSciences estimates (i.e., 2025 million hectares), and by all accounts, will continue to rise rapidly for several years.

The most critical concern of 2,4-D is drift problem. It has caused a lot of damage to off-site locations, endangered species, and non-target crops, as well as to people who live near application sites (Nichelle Harriott, 2014). Typically, spraying during windy conditions and using nozzles that create fine spray droplets increase the risk of spray drift. High temperatures and low volatility also increase the risk of drift. Many forms of 2,4-D volatilize above $29\,^{\circ}\mathrm{C}$, and drift has been known to damage specialty crops such as soybeans and grapes (Figure 1.8) $0.8\,\mathrm{km}$ or more from the application site, even at concentrations 100 times below the recommended label rate (Anon, 2015). The volatilization rates of 2,4-D are determined by the temperature and formulation of the herbicide at the surface of the soil (Mccall et al., 1981). In general, dry, alkaline soils with high organic content will be less likely to lose 2,4-D to volatilization (Que Hee and Sutherland, 1974; Anon, 2015).

Figure 1.8: (a)The common symptoms of 2,4-D injuries on soybeans often include the curling and cupping of the leaf (Cowbrough, 2011), (b)2,4-D injury symptoms on grape shoots often include a cessation of shoot tip growth and an abundance of lateral shoots (Muza, 2015).

The half-life of 2,4-D in the environment is relatively short, averaging ten days in soils and less than ten days in water, but can last significantly longer in cold, dry soils, or where the appropriate microbial community is not present to promote degradation (Wager, 2017). 2,4-D degrades fairly quickly in soils, and microbial degradation is considered to be the major route in the breakdown of the 2,4-D in the soil, but it is relatively persistent in anaerobic aquatic environments (half-life ranges from 41 to 333 days) (USEPA, 2005). Although 2,4-D is highly mobile and it does not bind with minerals in soils (Organization, 1989), and has a high potential to leach from soil surface, it is less likely to contaminate groundwater due to its rapid degradation. The amine salts and ester forms are not persistent under most environmental conditions (Donald et al., 2001). 2, 4-D when applied to surface water is quickly distributed throughout the water body, with a half-life of approximately 1-3 weeks. Generally, the acid and amine salts are practically non-toxic to freshwater and marine

fish, but the butoxyethanol ester is highly toxic. 2,4-D and its salts and esters are predicted to pose minimal risk to pollinators, like the honey bee, and other beneficial insects (cic, 2011).

Genetically engineered (GE), herbicide resistant (HR) and insect-resistant crops have been remarkable commercial successes in the U.S.. Total pesticide use has been driven upward by $1.83 \times 10^8\,\mathrm{kg}$ in the U.S. (Anon, 2015). This increase represents, on average, an additional $0.21\,\mathrm{kg\,ha^{-1}}$ of pesticide active ingredient for every GE-trait hectare planted. The estimated overall increase of $1.83 \times 10^8\,\mathrm{kg}$ applied over the past 16 years represents about a $7\,\%$ increase in total pesticide use.

The US Department of Agriculture (USDA) approved a new generation of genetically modified crops that are resistant to 2,4-D in 2014 (Charles, 2014). As the availability of the new genetically engineered forms of crops tolerant to 2,4-D, more 2,4-D is allowed by the farmers to spray to the herbicide across agricultural regions, the volume of 2,4-D sprayed could drive herbicide usage upward by approximate $50\,\%$.

1.6 Soil Surface Energy Balance

The soil surface energy balance is associated with shortwave radiation incoming from the sun and reflected by the earth's surface, and longwave radiation emitted by earth's surface and radiated toward the surface by the atmosphere (Figure 1.9). The exchange of energy between the earth's surface and the overlying atmosphere involves several important processes (Douglas J. Parker, 2017), which are

1. Thermal conduction of heat energy within the ground.

2. Turbulent transfer of heat energy towards or away from the surface within the atmosphere.

3. Evaporation of water stored in the soil vapor onto the surface.

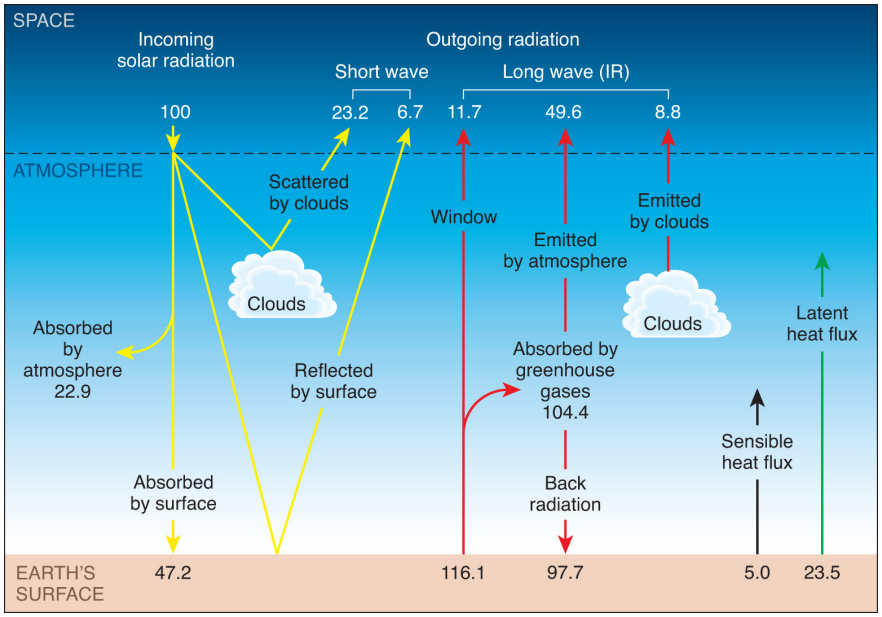

Figure 1.9: Earth's Radiation Balance (Youngman, 2017).

1.6.1 Atmosphere-Soil Interface

Soils are characterized by close coupling to atmosphere, lithosphere, biosphere and hydrosphere as neighboring systems. The soil surface conditions such as temperature and matric potential are directly influenced by the atmosphere. Incoming solar radiation forcing is predominantly daily periodic, leading to a similar strong periodicity within the soil atmospheric boundary layer system (Gentine et al., 2011). The daily cycle of incoming radiation at the land surface results in changes in the surface energy balance through the modification of outgoing radiative, turbulent, and soil heat fluxes. Annual and diurnal variations in ground temperaturecan be predicted with the energy balance equation (Deardorff, 1978), which essentially calculates the overall radiant energy being absorbed or emitted by the thin upper layer of the ground surface (Sedighi et al., 2016).

Soil-atmosphere exchange processes include net radiation, latent heat, sensible heat and ground heat fluxes. The Mollier diagram is a graphic representation of the relationship between air temperature, moisture content and enthalpy. It is useful when analyzing the performance of

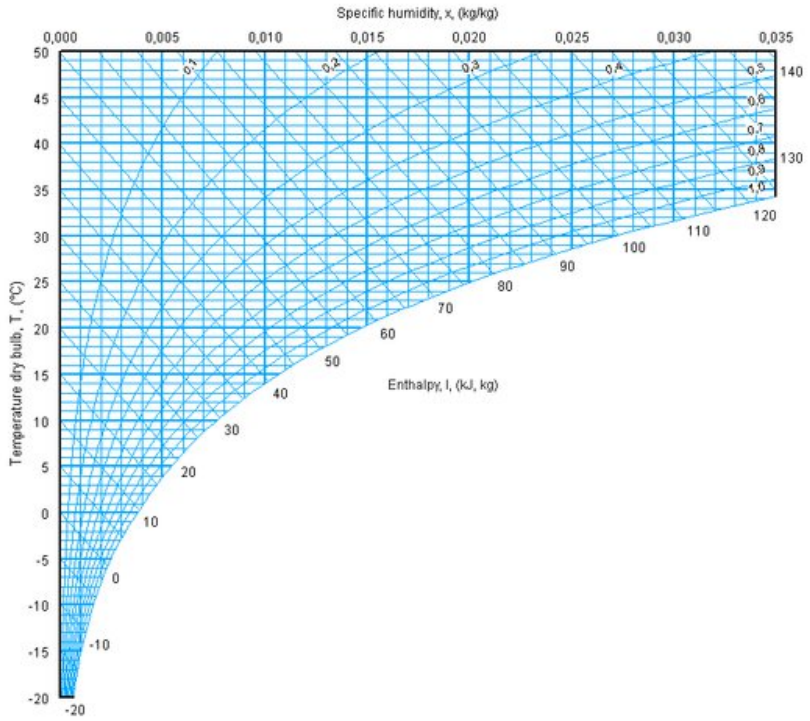

Figure 1.10: Mollier Diagram, it is a graphic representation of the relationship between air temperature, moisture content and enthalpy (Mollier, 2017).

adiabatic steady-flow processes, such as flow in nozzles, diffusers, turbines and compressors. A typical Mollier diagram is shown in Figure 1.10.

1.6.2 Modelling Coupled Transport

Temperature affects all physical, chemical and biological processes in soils. Reaction rates for many processes double for every $10\,^{\circ}\mathrm{C}$ increase in temperature(Connors, 1990). Physical processes, such as water movement and soil drying, are also strongly influenced by temperature (Marco Bittelli and Tomei, 2015).

Heat, water and vapor flow in soils are coupled, and the most important process determining the coupling between water and heat is the transport of latent heat by vapor flow within the soil and at the interface between soil and atmosphere (Marco Bittelli, 2008). Therefore, the programs for heat, water and water vapor must be linked to describe coupled transport. Accounting for different

transport processes is very important for a variety of applications. For instance, soil water content and soil temperature affect microbial transformation in soil, as well as the nitrogen and carbon cycles.

1.7 Objectives

The objectives of this study were to improve our understanding of herbicide fate in agroecosystem by determining how soil temperature, relative humidity, soil texture and soil mineralogy, affect 2,4-D volatilization.

My specific objectives were to:

1. Develop water vapor isotherms and calculate monolayer water contents for selected reference minerals and selected surface horizons collected from Alabama benchmark soils.
2. Determine the effect of relative humidity on 2,4-D volatilization.
3. Compare the specific surface area values of clay minerals from different prediction models.
4. Measure diurnal soil surface temperature cycles and determine the matric potential of the top soil layer.

Chapter 2

Theory

BET and GAB models are common mathematical functions that describe WSIs for various materials (Dogan et al., 2006; Fujita, 1963; Maroulis et al., 1988; Prothon and Ahrne, 2004). This chapter contains the equations to calculate the monolayer water content based on BET and GAB models as well as the specific surface area calculation.

2.1 Brunauer Emmett Teller Model

The BET model is firstly reported in 1938 (Brunauer et al., 1938), it is based on theory of statistical thermodynamics. BET model is based on the application of the Langmuir equation to the first and subsequent layers of adsorbate on the surface. In the BET model, the heat of adsorption of the second and following monolayers is assumed to be constant and equal to the heat of liquefaction. Two basic assumptions for the derivation of the BET equation are:

1. The surface of the adsorbent is homogeneous.

2. There is no lateral interaction between the adsorbed molecules.

BET equation:

$$p = \left[\frac{c-1}{m_0 c}\right] a_w + \frac{1}{m_0 c} \tag{2.1}$$

with

$$p = \frac{a_w}{(1-a_w)m} \tag{2.2}$$

Where a_w is the water activity ($a_w < 0.55$), m is the water content (dry basis), m_0 is the monolayer water content, c is energy constant, p is a parameter calculated by a_w and m . Due to the two basic

assumptions to derive the equation, BET model is only applicable when a_w is lower than 0.55. The monolayer water content can be calculated by the slope and intercept of the a_w vs p plot.

$$m_0 = \frac{1}{intercept + slope} \tag{2.3}$$

2.2 Guggenheim, Anderson and De Boer Model

The GAB model is a modified version of the BET model. Other than the BET model, the GAB model postulates that the heat of adsorption of the second and following monolayers is constant, but less than the heat of liquefaction (Louis B. Rockland, 1981), and the GAB model has one more parameter than BET. The GAB model is also a statistical thermodynamics basis theory. In general, the GAB equation is considered the most versatile due to its ability to cover a wider a_w range. The GAB model can be expressed by the following equation:

$$q = \frac{k}{m_0(\frac{1}{c} - 1)} a_w^2 + \frac{c-2}{m_0 c} a_w + \frac{1}{m_0 c k} \tag{2.4}$$

with

$$q = \frac{a_w}{m} \tag{2.5}$$

Where a_w is the water activity ($0.05 < a_w < 0.95$); m is the water content (dry basis); m_0 is the monolayer water content, c and k are energy constants, q is a parameter calculated by a_w and m.

To determine the monolayer water content by using GAB, a simple method was used which is straightforward (Timmermann, 2003), it uses the so-called transformed form of the GAB equation (Schaer, 1988), the following parabolic expression, which is easily derived from equation.

$$a_w/m = \alpha + \beta a_w + \gamma a_w^2 \tag{2.6}$$

$$\frac{a_w}{m} = \frac{k}{m_0(\frac{1}{c} - 1)} a_w^2 + \frac{c-2}{m_0 c} a_w + \frac{1}{m_0 c k} \tag{2.7}$$

where

$$\alpha = \frac{1}{m_0 c k} \tag{2.8}$$

$$\beta = \frac{c-2}{m_0 c} \tag{2.9}$$

$$\gamma = \frac{(1-c) \times k}{m_0 c} \tag{2.10}$$

The three constants α, β and γ are determined by a least-square regression of this second degree polynomial and from these, the three GAB constants are calculated by,

$$k = \frac{\sqrt{(}\lambda) - \beta}{2\alpha} \tag{2.11}$$

$$m_0 = \frac{1}{\sqrt{(}\lambda)} = \frac{1}{\beta + 2k\alpha} = \frac{k}{k^2\alpha - \gamma} \tag{2.12}$$

$$c = 1 - \frac{\gamma}{k^2\alpha} = 2 + \frac{\beta}{k\alpha} = \frac{1}{k\alpha\sqrt{(}\lambda)} \tag{2.13}$$

where

$$\lambda = \beta^2 - 4\alpha\gamma \tag{2.14}$$

2.3 Specific Surface Area Calculation

Specific Surface Area is one of the most significant characteristics of soil and sediments (Catherine N. Mulligan, 2009), and it is well known that the SSA of soil is influenced by the mineral type and content (Bingham et al., 1978), organic matter content (Feller, 1992), the degree

of inter-particle association (Schulze and Schwertmann, 1984), and also the average size of the particles (Schwertmann, 1985). Since m_0 is directly related to the SSA (Akin and Likos, 2014), it is also influenced by these factors. The SSA can be calculated by the following equation:

$$SSA = \frac{m_0}{m_w} \times N \times A \tag{2.15}$$

In which m_w is the molecular mass of water (0.018 kg mol^{-1}), N is the Avogadro$'$s number (6.023 $\times$ 10^{23} mol^{-1}), A is the area covered by one H_2O molecule ($A = 10.8\times$ 10^{-8}m^2).

Chapter 3

Materials and Methods

3.1 Development of Water Vapor Sorption Isotherms and Step Isotherms

The water vapor sorption isotherms and step isotherms were measured with the fully automatic AquaLab VSA (Meter Environment Inc., Pullman, WA, USA). The VSA measures both Dynamic Vapor Sorption (DVS) and Dynamic Dew point Isotherm (DDI) isotherms. The DVS method for equilibrium isotherms consists of tracking sample weight as the sample is exposed to different controlled humidity levels. The sample is held at each humidity level for a preset time interval. Once equilibrium is achieved, the instrument dynamically steps to the next preset humidity level. The DVS method works well for investigating the kinetics of sorption, what happens to a medium as it is exposed to certain humidity and how fast it adsorbs or desorbs water. The DVS method is not very helpful in creating a high-resolution isotherm curve, however, the DDI method is designed to solve this problem. The DDI method for dynamic isotherms is a water activity and gravimetric analysis method that controls neither water content nor water activity, but dries or wets the sample and measures water activity and water content during the wetting or drying process. It creates high-resolution isotherms that show detail in the adsorption and desorption curves by taking a snapshot of both water activity and water content as the sample is exposed to humidified or desiccated air.

Water adsorption and desorption isotherms were measured with the VSA using DDI method. An approximately $2\,\mathrm{g}$ air-dried medium sample was used without any pre-treatment. In brief, the VSA dries or wets an initially air-dry soil sample and automatically measures the water potential with a chilled-mirror dew point technique (Leong et al., 2003; Campbell et al., 2008) while simultaneously recording the sample mass throughout the drying or wetting process with a

high-precision magnetic balance. The following instrumental settings were used for water vapor sorption isotherm measurements: isotherm measurement mode; Dynamic Dew point Isotherm (DDI); RH range, $3\,\%$ to $95\,\%$; data resolution, $2\,\%$ RH; temperature, $25\,^{\circ}\mathrm{C}$; loop, on. After the conclusion of the measurements, samples were oven-dried for $48\,\mathrm{h}$ to determine the reference oven-dry water contents. Completely adsorption and desorption loops typically took $24\,\mathrm{h}$ to $72\,\mathrm{h}$.

Step isotherms were measured with the VSA using the DVS method. The step isotherm was developed for RH values of $5\,\%$, $15\,\%$, $25\,\%$, $35\,\%$, $45\,\%$, $55\,\%$, $65\,\%$, $75\,\%$, $85\,\%$ and $95\,\%$. At each RH stage the medium was allowed to equilibrate for $2\,\mathrm{h}$. Step isotherm were then used to calculate the monolayer water content of the test medium by using both BET (Section 2.1) and GAB equations (Section 2.2).

3.2 Clay Minerals and Benchmark Soils

The need for sources of homogeneous clay samples had become apparent to researchers since the early 1970's. Natural deposits are very variable that data generated by different investigators working at the same outcrop often cannot be compared with confidence. Therefore the Clay Minerals Society set up the Source Clays Project (Moll, 2002). The Clay Minerals Society source clay minerals include for example kaolinite, hectorite, montmorillonite, synthetic mica-montmorillonite, palygorskite (Costanzo, 2001). Many properties of these source clays have

Table 3.1: Mineralogy and Locations of the Special Clays from The Clay Minerals Society.

Special Clay	Mineralogy	Location
KGa-2	Kaolinite	Warren, GA
KGa-1b	Kaolinite	Washington, GA
ISCz-1	Illite-Smectite	Czechoslovakia
SAz-1	Montmorillonite	Apache, AZ
SWy-3	Na-Rich Montmorillonite	Crook, WY
STx-1b	Ca-Rich Montmorillonite	Gonzales, TX
Syn-1	Synthetic Mica-Montmorillonite	NL Industries
SHCa-1	Hectorite	San Bernardino, CA
PFI-1	Play-Gorskite	Gadsden, FL

been studied, including geological origin (Moll, 2001), chemical analyses (Mermut and Lagaly, 2001), layer-charge determination (Mermut and Lagaly, 2001), powder X-ray diffraction (Chipera D. L. et al., 2001), infrared spectra (Madejova and Komadel, 2001), thermal analyses (Guggenheim and van Groos, 2001), cation exchange capacities (Chipera D. L. et al., 2001), colloidal and surface properties (Wu, 2001) and the specific surface area (Dogan et al., 2006).

Several source clay minerals and benchmark soils from Alabama were used in this study. Nine clay minerals were obtained from the Clay Mineral Society (The Clay Mineral Society, VA, USA), the mineralogy and locations of the clay minerals can be found in Table 3.1.

The benchmark soils were a Cecil soil from a Bt2 horizon, a Dothan soil from a Bt2 horizon and an Orangeburg soil from a Bt3 horizon. The B horizon is the subsoil layer that generally changes the most because of the soil forming processes , the "t" stands for "translocated clay". The Bt horizon has more clay in them than the horizons below and above them. The soil samples from Bt horizon were used in this study because with higher clay content, it is easier to compare benchmark soils with source clay minerals, and it is more representative than the soil samples from the other horizon. Soil samples were air dried and then sieved by No.60 mesh ($250\,\mu\mathrm{m}$) prior to processing in the VSA.

3.3 2,4-D Application

The formulation used in this study was 2,4-D amine with $47.3\,\%$ active ingredient (Dimethyl amine salt of 2,4-D acid) (Figure 3.1) and $52.7\,\%$ other inactive ingredients. The chemical properties of 2,4-D amine can be found in Table 3.2.

Table 3.2: 2,4-D Amine Chemical Properties.

Formulation	Solubility[1] (mg/L)	Vapor Pressure[2](kPa)	Half-Life	Application Season
Amine	700,000	1×1.33^{-9}	1 to 2 weeks	Spring/summer

[1]Solubility in water given for unbuffered solution.
[2]Vapor pressure measured at $25\,^{\circ}\mathrm{C}$

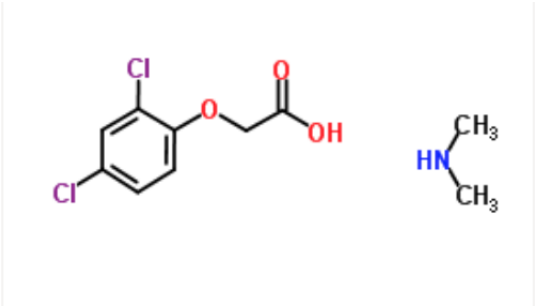

Figure 3.1: The Chemical Structure of 2,4-D dimethylamine.

The common application amount of commercial 2,4-D amine product is $185\,\mathrm{L\,ha^{-1}}$ water solution with an active ingredient application rate of $2.24\,\mathrm{kg\,ha^{-1}}$. To prepare the application solution, $0.1\,\mathrm{g}$ of commercial 2,4-D amine product was diluted in $10\,\mathrm{mL}$ of deionized water (DI water). The concentration of the final application solution was $10\,\mathrm{mg\,mL^{-1}}$. The application solution was stored in the refrigerator and was used within 4 weeks. $20\,\mu\mathrm{L}$ of application solution was applied to each test medium, which was the same as the field application rate. The application of the 2,4-D amine solution was done with a pipette ($10\,\mu\mathrm{L}$ to $100\,\mu\mathrm{L}$). Before applying the herbicide, the test medium was equilibrated for $24\,\mathrm{h}$ under the same RH and temperature condition as the experiment setting.

3.4 Volatilization Experiments

A VSA sample cup was filled with about $2.0\,\mathrm{g}$ of the test medium (Figure 3.2). The herbicide was then mixed with water and applied to the test medium at the rate of $2.24\,\mathrm{kg\,ha^{-1}}$ with a pipette. The sample cup was placed immediately into the VSA and exposed to four different relative humidity regimes, in which two of them were higher than m_0-RH and the other two were lower. After that, the 2,4-D residues were extracted from the soil by adding extraction solution, which is a mixture of High Performance Liquid Chromatography (HPLC) grade methanol and $96\,\%$ phosphoric acid (9:1). After shaking for $2\,\mathrm{h}$, centrifuged the samples at 3000RPM for $10\,\mathrm{min}$, the supernatant was kept and filtered by $100\,\mu\mathrm{m}$ filter (Figure 3.3). Finally, the High Performance Liquid Chromatography (HPLC) was used to measure the 2,4-D

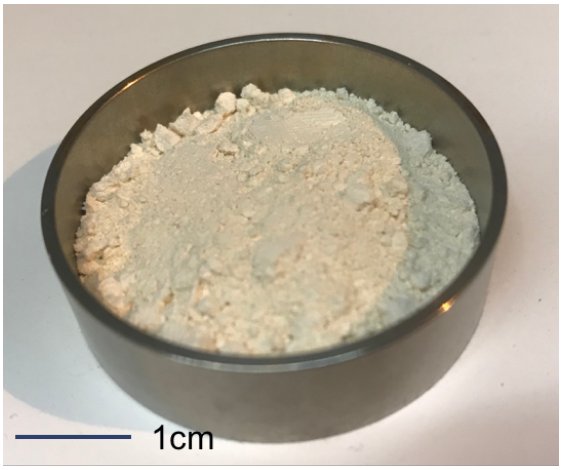

Figure 3.2: The Sample Can of Vapor Sorption Analyzer with Test Medium.

concentration of the extraction solution. The mobile phase of HPLC consisted of a mixture of acetonitrile and $10\,\mathrm{mmol}$ H_3PO_4 (50:50, v/v). The detection column is a 2.1 x 50mm C18 column. To optimize the HPLC parameters, the conditions were monitored by varying the flow rates and the detection wavelength. It was finally observed that the maximum absorbance of the 2,4-D amine and best selectivity of the peak was at the detection wavelength of $228\,\mathrm{nm}$, flow rate of $0.5\,\mathrm{mL/\,min}$ and $10\,\mu\mathrm{L}$ of injection (Table 3.4). Volatilized amount of 2,4-D was calculated via a mass balance between the amount of 2,4-D added to the medium (C_0) and the amount of 2,4-D that was extracted after the experiment (C):

$$VolatilizationRate = \frac{C_0 - \frac{C}{x}}{C_0} \times 100 \tag{3.1}$$

In which x is the extraction efficiency of each test media, we divided the C by x to account for different test media.

To determine the extraction efficiency, a recovery test was conducted. Three of $2.0\,\mathrm{g}$ of each test media were weighed in a $25\,\mathrm{mL}$ screw-capped centrifuge tube, $20\,\mu\mathrm{L}$ of the 2,4-D application solution was added to each tube, and then $20\,\mathrm{mL}$ of extraction solution was added and the tubes were shaken by a mechanical shaker for $2\,\mathrm{h}$, the tubes were centrifuged after shaken, the supernatant was kept and measured with HPLC, the extraction efficiency (x) was calculated by

Figure 3.3: 2,4-D Extraction Method.

Table 3.3: 2,4-D Extraction Efficiency of All Test Media (n=3).

Minerals	Extraction Efficiency $\pm$ Standard Error (%)
Kaolinite	76.68 ± 1.74
Illite-Smectite	72.70 ± 0.98
Na-Rich Montmorillonite	75.60 ± 4.37
Ca-Rich Montmorillonite	84.43 ± 1.88
Dothan	88.87 ± 4.61
Cecil	80.96 ± 2.23

comparing the added 2,4-D amount (C_0) and the 2,4-D residue amount (C) that quantified by HPLC:

$$x = \frac{C}{C_0} \times 100 \tag{3.2}$$

The extraction efficiency of all the test media can be found in Table 3.3.

The calibration curve was obtained by duplicate analysis of each 2,4-D amine standard solutions at five concentration levels ranged between $5\,\mathrm{mg\,L^{-1}}$ and $50\,\mathrm{mg\,L^{-1}}$, which were $5\,\mathrm{mg\,L^{-1}}$, $10\,\mathrm{mg\,L^{-1}}$, $15\,\mathrm{mg\,L^{-1}}$, $30\,\mathrm{mg\,L^{-1}}$, $40\,\mathrm{mg\,L^{-1}}$ and $50\,\mathrm{mg\,L^{-1}}$. The standard solutions were spiked by dilution of the 2,4-D application solution. The standard solutions were measured along with the samples for volatilization experiments under the same HPLC conditions.

3.5 Soil and Weather Data Collection

I monitored the soil surface temperature, soil temperature, soil water content, and soil matric potential in two depths ($5\,\mathrm{cm}$ and $10\,\mathrm{cm}$) using Degacon sensors and data loggers (infrared

Table 3.4: Chromatographic Conditions (HPLC-UV) Used for Detection of 2,4-D Amine.

Parameters	Details
Mobile Phase	ACN-H_3PO_4 (50:50)
Flow Rate	$0.5\,\mathrm{mL/\,min}$
Temperature	$25\,^{\circ}\mathrm{C}$
Detection Column	C18
Injection Volume	$10\,\mathrm{mL}$
Detection Wavelength	$228\,\mathrm{nm}$

thermometer, 5TE soil water content sensor, MPS-6 soil matric potential sensor, and EM50 data logger, Meter Environment, Pullman, WA). These measurements were taken in the vicinity of a weather station to be able to relate soil surface to air temperature on the experimental fields on campus (Auburn University). Additionally, I took surface soil samples at typical 2,4-D application times at April 15th, 2017. The hourly weather data was provided by AWIS Weather Service (Services, 2017), which included air temperature, relative humidity, precipitation amount, solar radiation, wind speed and wind direction.

3.6 Soil Surface Energy Balance Modeling

The soil-atmosphere interface is complex. The soil surface temperature usually experiences a higher temperature amplitude in comparison to the air temperature. Higher soil surface temperature also increases the saturated vapor pressure. I simulated the soil surface relative humidity and temperature conditions to determine the 2,4-D volatilization situation in the daily cycle.

3.6.1 Determination of Soil Surface Parameters

HYPROP (Meter Environment, Inc., Pullman, WA) is a modular lab instrument (Figure 3.4) that generates a moisture characteristic curve and determines the unsaturated hydraulic conductivity of soil samples in standard $250\,\mathrm{mL}$ soil sampling rings (Meter Environment, 2015). Two precision mini-tensiometers measure water potential at different levels within the sample while the sample rests on a precision laboratory scale ($2000\,\mathrm{g}$ range; $0.01\,\mathrm{g}$ resolution). As the

(a) HYPROP sample rings cutout.

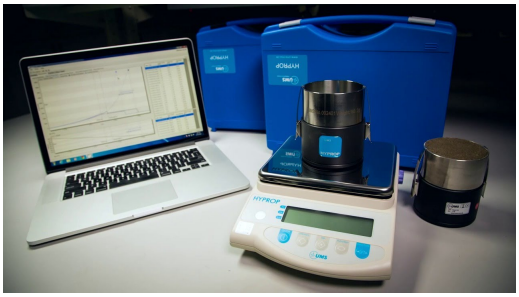

(b) HYPROP scale.

Figure 3.4: HYPROP (Meter Environment, 2015).

sample dries, changes in water potential are correlated to changes in moisture content using the Wind/Schindler evaporation method. Results were verified and values for dry range and saturation are calculated according to a selected model (i.e., van Genuchten/Mualem, Bimodal van Genuchten/Mualem, or Brooks and Corey.). Model parameters can be selected before, during, or after the measurement procedure.

Undisturbed soil was sampled from the weather station on Auburn campus, the soil texture is loamy sand, which was determined by texture analysis test. The soil parameters such as saturated conductivity (Ksat, m s^{-1}), soil residual water content (θ_r, m^3 m^{-3}), volumetric saturated water content (θ_s, m^3 m^{-3}) and empirical parameter for surface tension dependence on temperature (n) can be obtained by using HYPROP.

3.6.2 Simulation of Daily Cycles

Python 2.6 was used to simulate daily relative humidity and temperature cycle along with the weather data obtained from AWIS weather service and soil properties. The weather data of April 14, 2017 was used in this study. The Campbell and van Genuchten parameters were required by the daily cycle simulation. The Campbell and van Genuchten equations were used to describe the soil water retention curve. The soil water retention curve properties for Campbell$'$ equation such as Campbell water retention curve parameter (b), Campbell$'$s air-entry potential (ψ_e, J kg^{-1}) and volumetric saturated water content (θ_s, m^3 m^{-3}) were derived from W. J. Rawls (1982) (Table 3.5).

Osmotic coefficient (α, m^{-1} or kg J^{-1}), empirical parameter for surface tension dependence on

Table 3.5: Soil Water Retention Curve Parameters for Campbell′s Equation (W. J. Rawls, 1982).

Textural Class	b	ψ_e (J kg^{-1})	θ_s (m^3 m^{-3})
Loamy sand	2.11	-0.87	0.38

temperature (n), residual water content from van Genuchten′s equation (θ_s, m^3 m^{-3}) can be found in Marco Bittelli and Tomei (2015) (Table 3.6).

Table 3.6: Soil Water Retention Curve Parameters for van Genuchten′s Equation.

Textural Class	α (kg J^{-1})	n	ψ_e (J kg^{-1})	θ_r (m^3 m^{-3})	θ_s (m^3 m^{-3})
Loamy sand	0.49	1.5	-1.1	0.03	0.39

3.7 Data Analysis

Rstudio was used in the study for data analysis. The water vapor sorption isotherms and step isotherms were generated by Rstudio using the package ggplot2, and the monolayer water content and specific surface area were then calculated by Rstudio. Three-way linear regression was conducted for the 2,4-D volatilization experiment analysis at 95% confidence interval, monolayer water content, relative humidity and media were the variables and the 2,4-D volatilization rate was the response variable. The daily temperature and relative humidity cycles were generated by using ggplot2 as well.

Chapter 4

Results and Discussion

4.1 Monolayer Water Content Calculations using BET and GAB Theory

The monolayer water content of a soil is the soil water content when the soil is covered by only one layer of water molecules. The monolayer water content of all the clay minerals and benchmark soils was calculated by both BET and GAB equations with the H_2O sorption isotherm. The BET plots and GAB plots for the test media are given in Figures 4.3 to 4.14 and Figures 4.15 to 4.26. Two BET equations and two GAB equations were obtained for each clay and two monolayer water contents for each model were averaged. The BET model based m_0 used a shorter relative humidity range ($5\,\%$ to $35\,\%$), while the GAB model using the whole RH range. The results were reported in Table 4.1. Figure 4.1 is a direct comparison of monolayer water content for all test media estimated from BET model and GAB model.

The BET based monolayer water content values range from $0.50\,\%$ to $6.01\,\%$, and the GAB based monolayer water content values range from $0.82\,\%$ to $7.37\,\%$. The commonly used BET equation gives the lower monolayer water content values compared with GAB. Monolayer water content values calculated from GAB-based exceed the BET-based values by about $21.6\,\%$ to $233.3\,\%$over the entire measured range. The relation between the monolayer water content of all the test media from BET and GAB can be expressed by the following equation (R^2=0.95):

$$m_0GAB = 1.24 \times m_0BET + 0.47 \tag{4.1}$$

with

$$R^2 = 0.95 \tag{4.2}$$

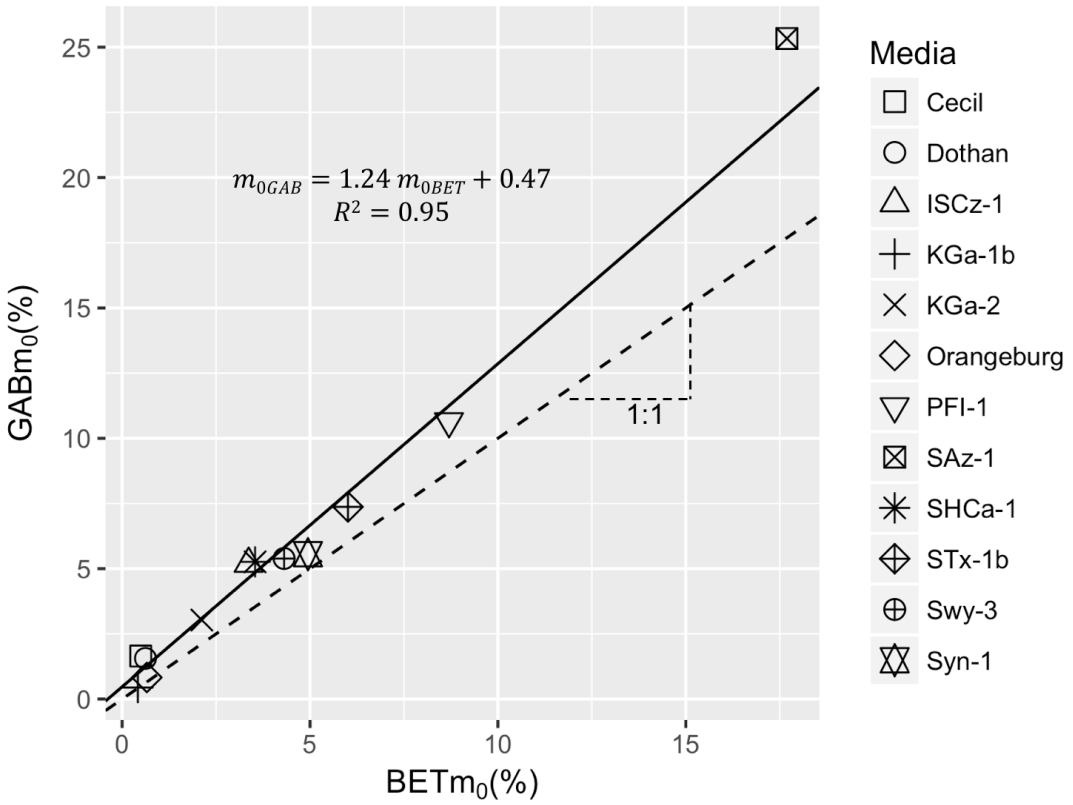

Figure 4.1: Soil Monolayer Water Content from BET and GAB Models.

Table 4.1: Monolayer Water Content of Studied Media from both BET and GAB models, SE indicates the Standard Error (n=2).

Type	Media	BET-m_0 (%) ± SE(%)	GAB-m_0 (%) ± SE(%)
Clay Minerals	KGa-1b	0.42 ± 0.03	0.44 ± 0.03
	KGa-2	0.57 ± 0.00	0.63 ± 0.00
	ISCz-1	2.70 ± 0.69	4.12 ± 0.31
	SHCa-1	3.54 ± 0.64	5.26 ± 0.11
	SWy-3	4.15 ± 0.37	5.32 ± 0.37
	SYn-1	4.95 ± 1.09	5.56 ± 1.22
	STx-1b	6.01 ± 1.64	7.38 ± 1.82
	PFI-1	8.70 ± 2.61	10.65 ± 3.10
	SAz-1	17.69 ± 6.06	25.33 ± 6.85
Benchmark Soils	Orangeburg	0.74 ± 0.03	0.91 ± 0.08
	Dothan	0.74 ± 0.01	1.28 ± 0.28
	Cecil	0.6 4± 0.01	1.25 ± 0.41

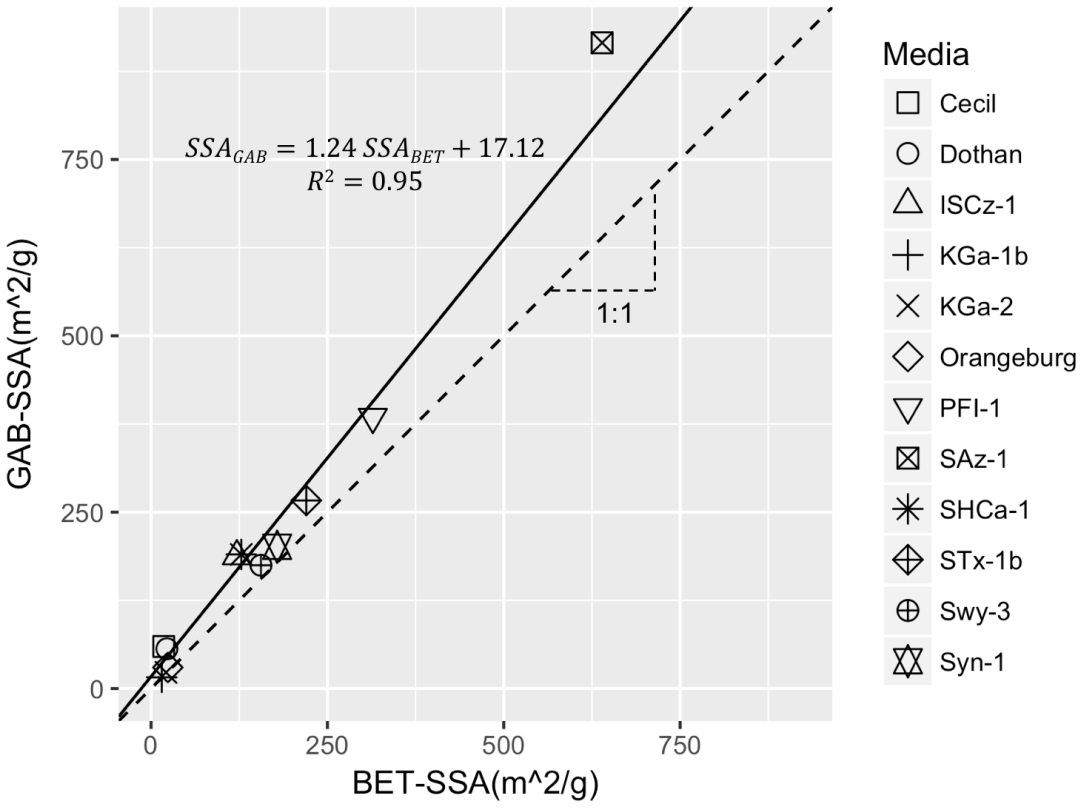

Figure 4.2: Specific Surface Area Values from BET and GAB Models.

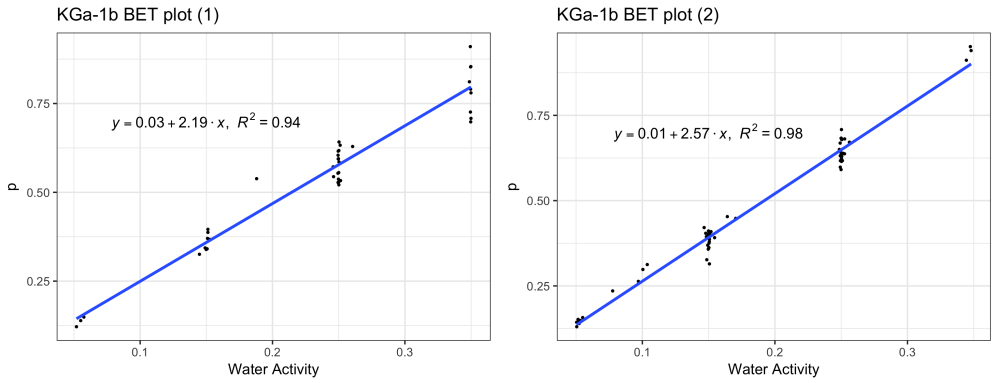

Figure 4.3: Monolayer Water Content Measurements of Kaolinite (KGa-1b) from The Clay Minerals Society by Using BET Model, in Which x Axis is Water Activity, y Equals to $a_w/(1-a_w)m$, see Equation (2.2).

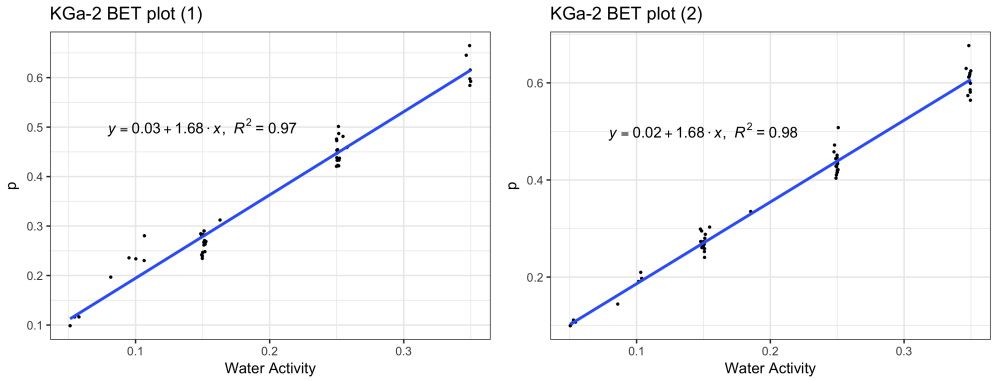

Figure 4.4: Monolayer Water Content Measurements of Kaolinite (KGa-2) from The Clay Minerals Society by Using BET Model, in Which x Axis is Water Activity, y Equals to $a_w/(1-a_w)m$, see Equation (2.2).

Dogan et al. (2007) conducted a baseline study among the SSA of the source clay minerals by using BET model. The SSA of the seven source clay minerals were 13.1, 21.7, 35.6, 65.2, 22.7, 118 and $173\,\mathrm{m^2\,g^{-1}}$. Compared with the results from Dogan et al. (2007), the SSA obtained from BET model in this studied are higher. The reason could be that we used a more advanced instrument which is VSA in this study, the sorption isotherm obtained from the VSA is more accurate and has a higher resolution than the sorption isotherm in Dogan et al. (2007) which was a traditional method. Four clay minerals which are KGa-2, SWy-3, STx-1b and ISCz-1 and three benchmark soils were selected as the test media for the 2,4-D volatilization experiment.

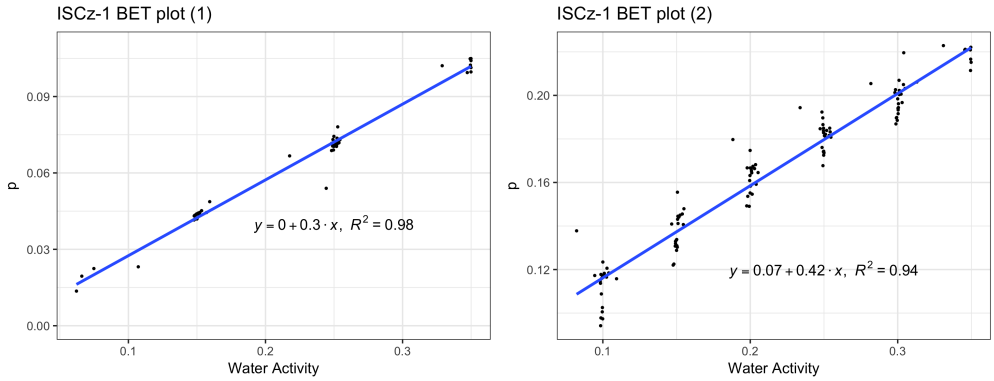

Figure 4.5: Monolayer Water Content Measurements of Smectite (ISCz-1) from The Clay Minerals Society by Using BET Model, in Which x Axis is Water Activity, y Equals to $a_w/(1-a_w)m$, see Equation (2.2).

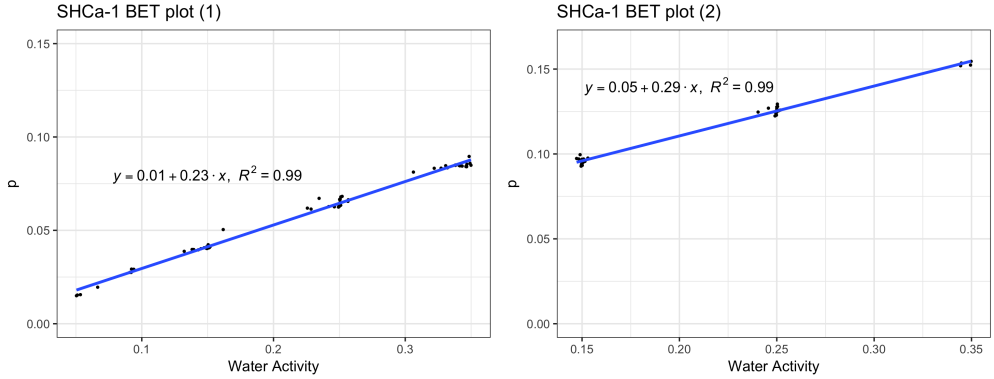

Figure 4.6: Monolayer Water Content Measurements of Hectorite (SHCa-1) from The Clay Minerals Society by Using BET Model, in Which x Axis is Water Activity, y Equals to $a_w/(1-a_w)m$, see Equation (2.2).

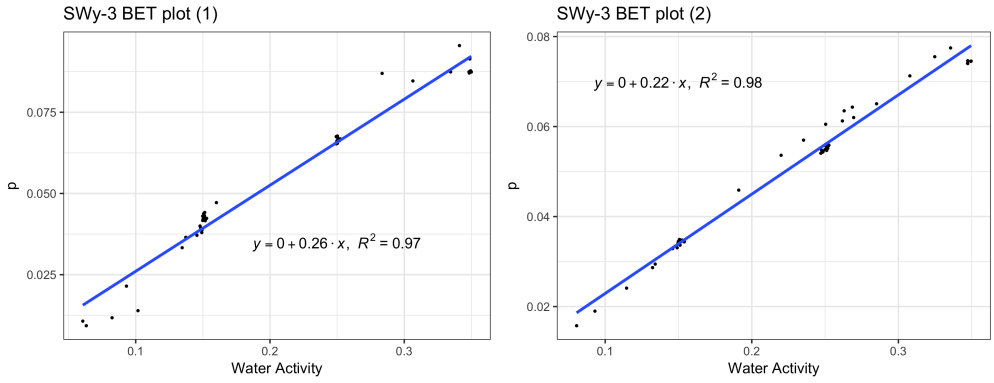

Figure 4.7: Monolayer Water Content Measurements of Na rich Montmorillonite (SWy-3) from The Clay Minerals Society by Using BET Model, in Which x Axis is Water Activity, y Equals to $a_w/(1-a_w)m$, see Equation (2.2).

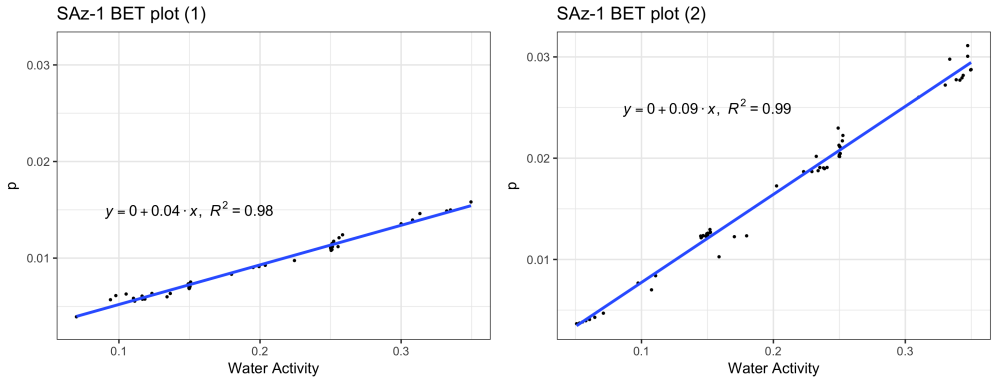

Figure 4.8: Monolayer Water Content Measurements of Montmorillonite (SAz-1) from The Clay Minerals Society by Using BET Model, in Which x Axis is Water Activity, y Equals to $a_w/(1-a_w)m$, see Equation (2.2).

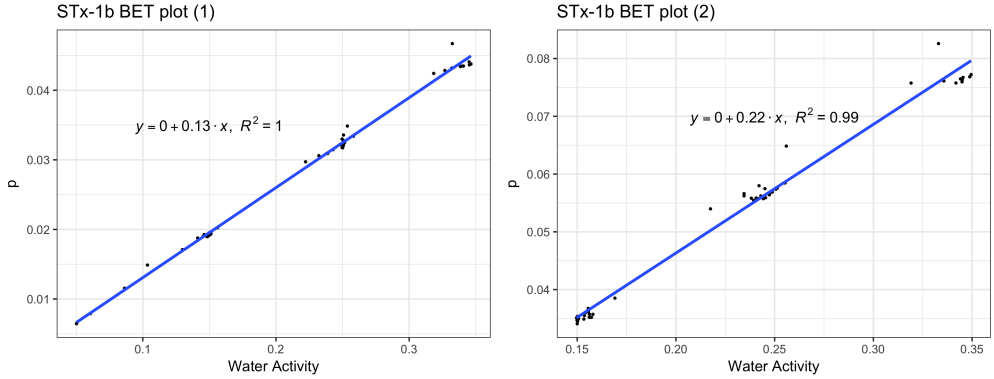

Figure 4.9: Monolayer Water Content Measurements of Montmorillonite (STx-1b) from The Clay Minerals Society by Using BET Model, in Which x Axis is Water Activity, y Equals to $a_w/(1-a_w)m$, see Equation (2.2).

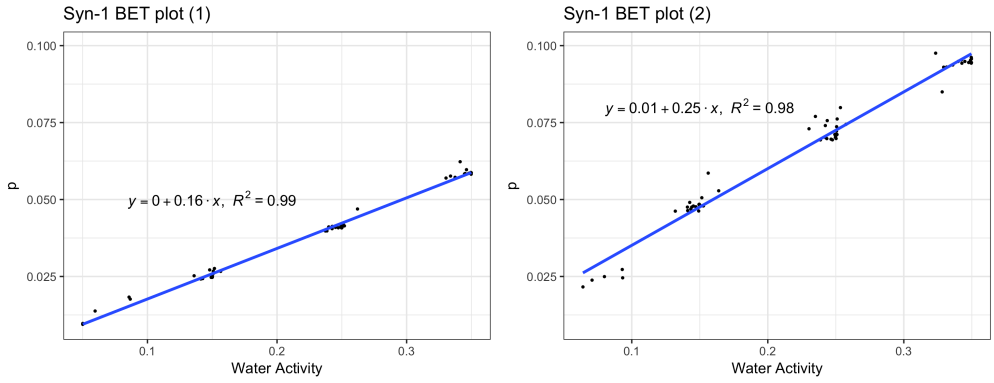

Figure 4.10: Monolayer Water Content Measurements of Synthetic Mica-Montmorillonite (SYn-1) from The Clay Minerals Society by Using BET Model, in Which x Axis is Water Activity, y Equals to $a_w/(1-a_w)m$, see Equation (2.2).

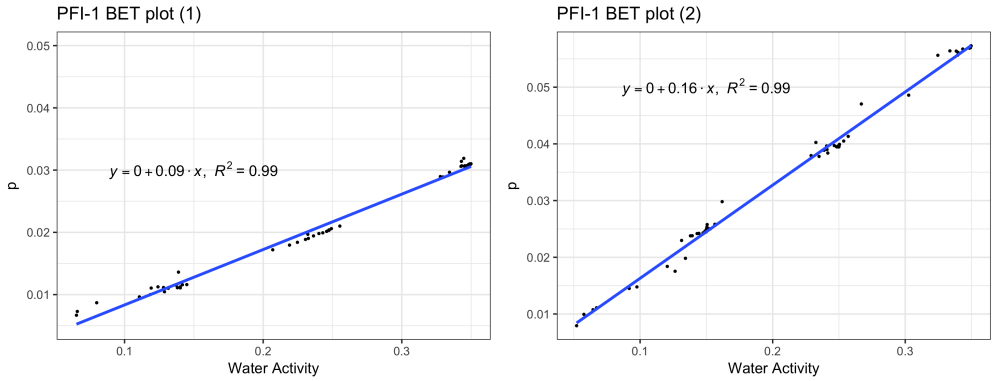

Figure 4.11: Monolayer Water Content Measurements of Palygorskite (PFl-1) from The Clay Minerals Society by Using BET Model, in Which x Axis is Water Activity, y Equals to $a_w/(1-a_w)m$, see Equation (2.2).

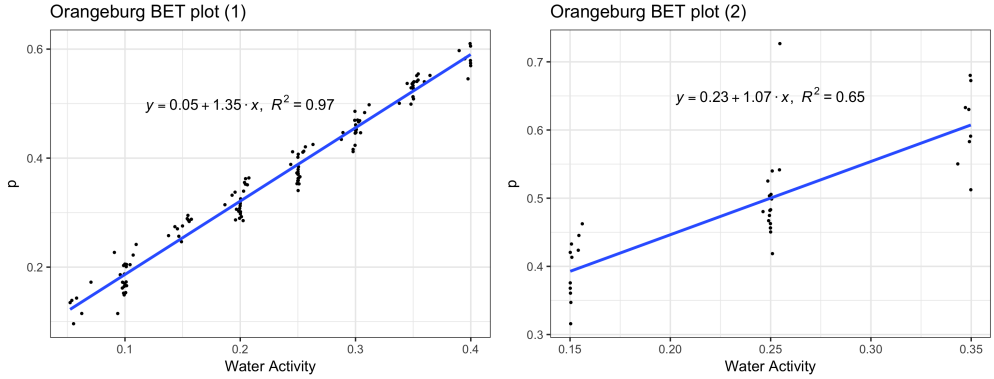

Figure 4.12: Monolayer Water Content Measurements of Orangeburg Soil from The Clay Minerals Society by Using BET Model, in Which x Axis is Water Activity, y Equals to $a_w/(1-a_w)m$, see Equation (2.2).

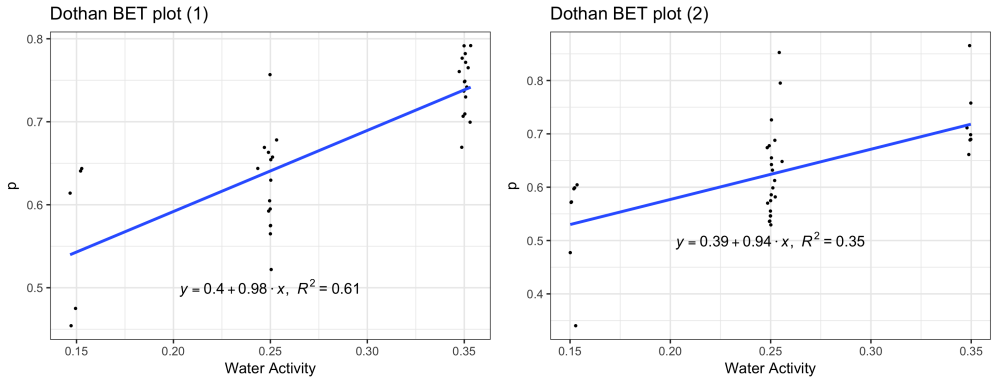

Figure 4.13: Monolayer Water Content Measurements of Dothan Soil from The Clay Minerals Society by Using BET Model, in Which x Axis is Water Activity, y Equals to $a_w/(1-a_w)m$, see Equation (2.2).

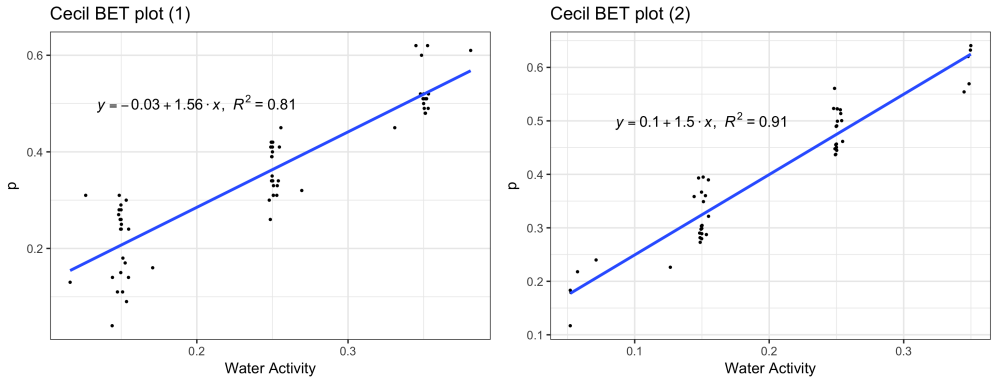

Figure 4.14: Monolayer Water Content Measurements of Cecil Soil from The Clay Minerals Society by Using BET Model, in Which x Axis is Water Activity, y Equals to $a_w/(1-a_w)m$, see Equation (2.2).

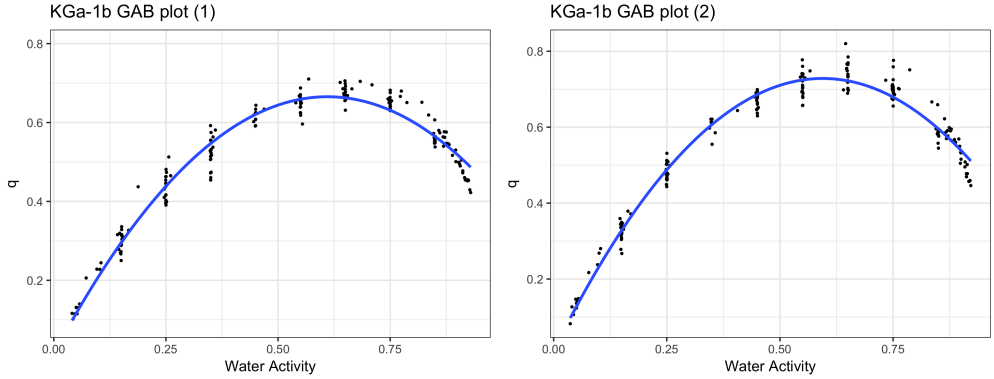

Figure 4.15: Monolayer Water Content Measurements of Kaolinite (KGa-1b) from The Clay Minerals Society by Using GAB Model, in Which x Axis is Water Activity, y Equals to a_w/m, see Equation (2.5).

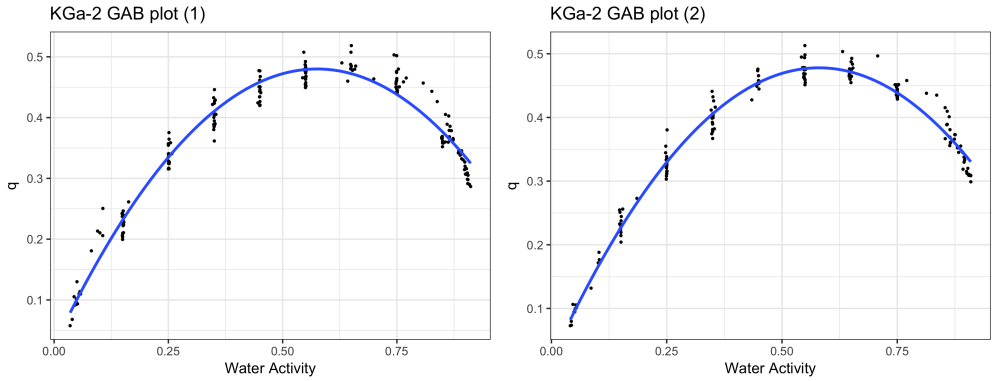

Figure 4.16: Monolayer Water Content Measurements of Kaolinite (KGa-2) from The Clay Minerals Society by Using GAB Model, in Which x Axis is Water Activity, y Equals to a_w/m, see Equation (2.5).

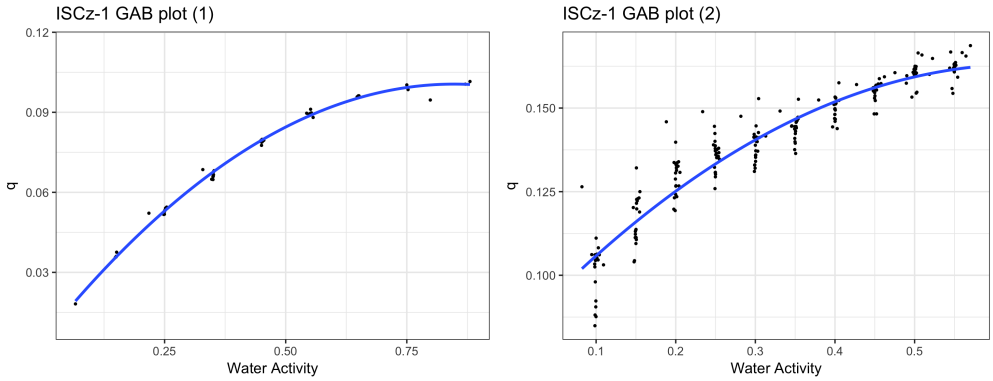

Figure 4.17: Monolayer Water Content Measurements of Smectite (ISCz-1) from The Clay Minerals Society by Using GAB Model, in Which x Axis is Water Activity, y Equals to a_w/m, see Equation (2.5).

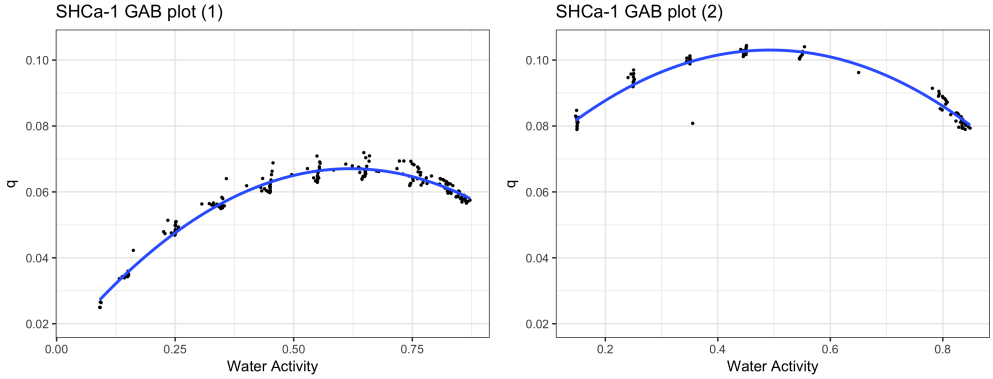

Figure 4.18: Monolayer Water Content Measurements of Hectorite (SHCa-1) from The Clay Minerals Society by Using GAB Model, in Which x Axis is Water Activity, y Equals to a_w/m, see Equation (2.5).

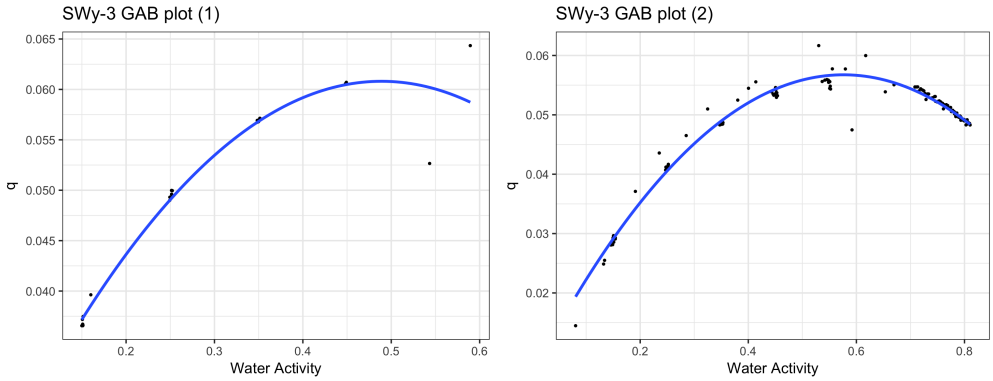

Figure 4.19: Monolayer Water Content Measurements of Na rich Montmorillonite (SWy-3) from The Clay Minerals Society by Using GAB Model, in Which x Axis is Water Activity, y Equals to a_w/m, see Equation (2.5).

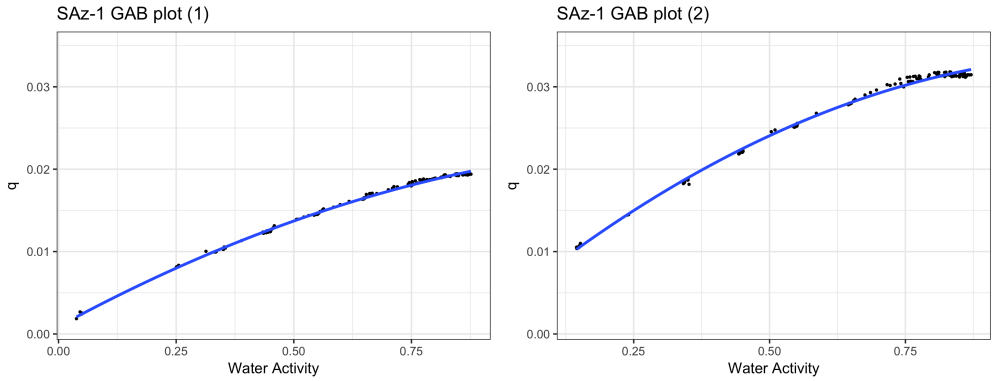

Figure 4.20: Monolayer Water Content Measurements of Montmorillonite (SAz-1) from The Clay Minerals Society by Using GAB Model, in Which x Axis is Water Activity, y Equals to a_w/m, see Equation (2.5).

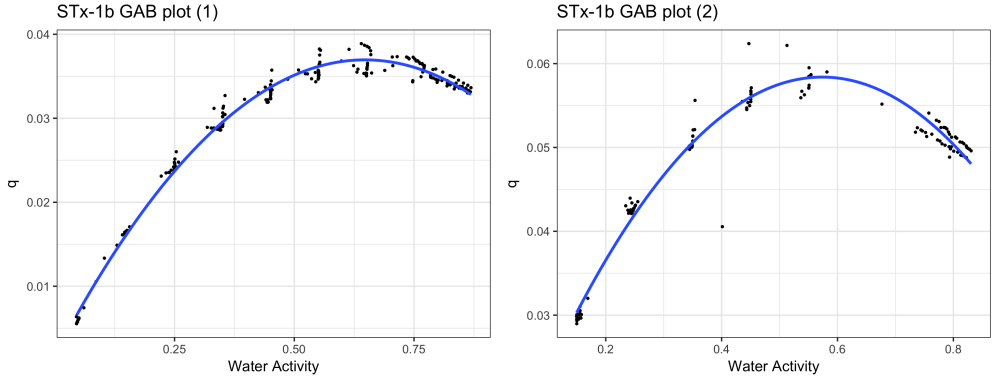

Figure 4.21: Monolayer Water Content Measurements of Montmorillonite (STx-1b) from The Clay Minerals Society by Using GAB Model, in Which x Axis is Water Activity, y Equals to a_w/m, see Equation (2.5).

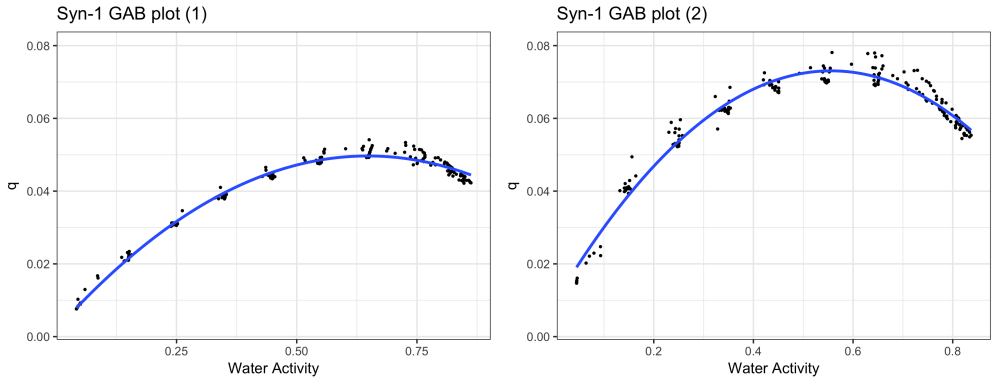

Figure 4.22: Monolayer Water Content Measurements of Synthetic Mica-Montmorillonite (SYn-1) from The Clay Minerals Society by Using GAB Model, in Which x Axis is Water Activity, y Equals to a_w/m, see Equation (2.5).

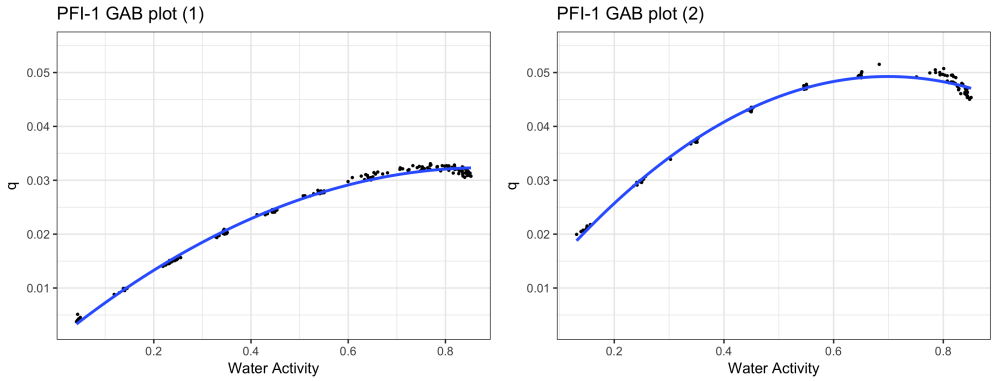

Figure 4.23: Monolayer Water Content Measurements of Palygorskite (PFl-1) from The Clay Minerals Society by Using GAB Model, in Which x Axis is Water Activity, y Equals to a_w/m, see Equation (2.5).

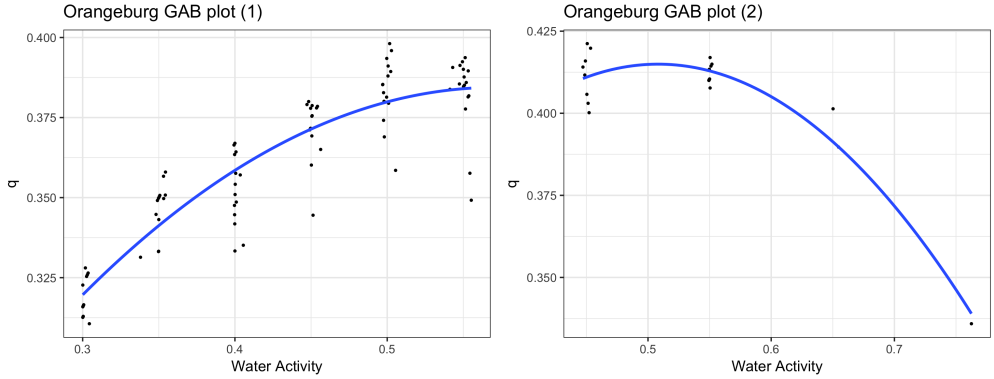

Figure 4.24: Monolayer Water Content Measurements of Orangeburg Soil from The Clay Minerals Society by Using GAB Model, in Which x Axis is Water Activity, y Equals to a_w/m, see Equation (2.5).

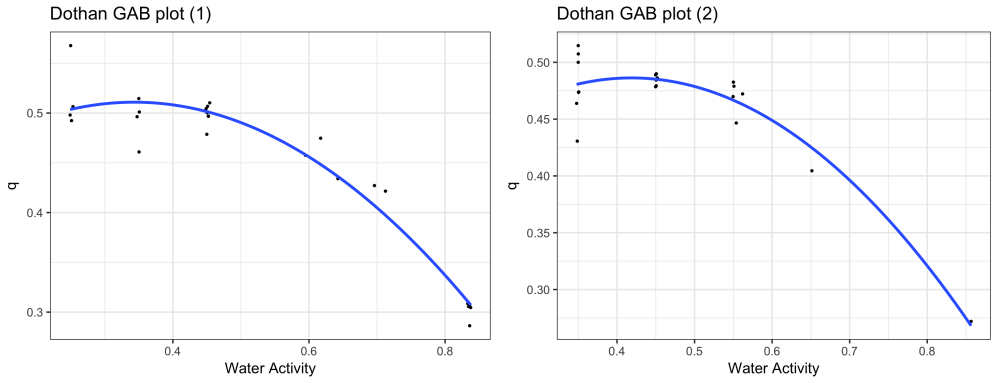

Figure 4.25: Monolayer Water Content Measurements of Dothan Soil from The Clay Minerals Society by Using GAB Model, in Which x Axis is Water Activity, y Equals to a_w/m, see Equation (2.5).

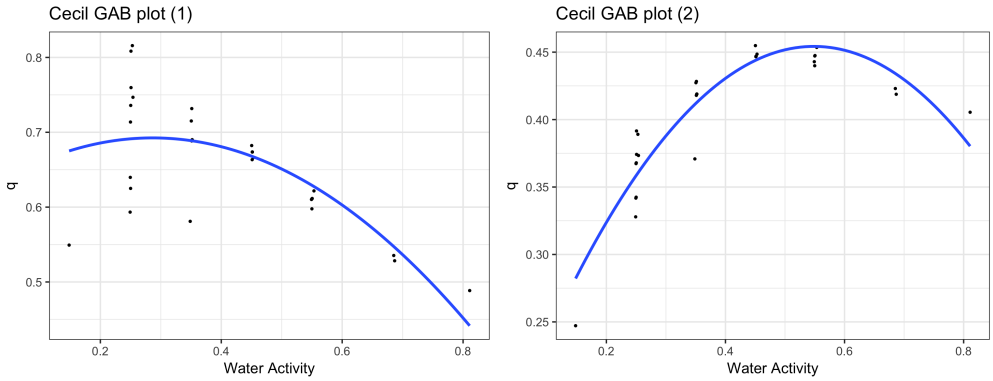

Figure 4.26: Monolayer Water Content Measurements of Cecil Soil from The Clay Minerals Society by Using GAB Model, in Which x Axis is Water Activity, y Equals to a_w/m, see Equation (2.5).

4.2 Specific Surface Area Calculations using BET and GAB Theory

The specific surface area values of all the clay minerals and benchmark soils were calculated by both BET and GAB equations as well as the H_2O sorption isotherm. The results were reported in table 4.2. The BET plots and GAB plots for the test media are given in Figures 4.3, 4.4, 4.6 and 4.8 to 4.11 and Figures 4.15, 4.16, 4.18 and 4.20 to 4.23. Two BET equations and two GAB equations were obtained for each clay and two specific surface area results for each model were averaged. Figure 4.2 is a direct comparison of SSA for all test media estimated from BET model and GAB model.

The BET based SSA values range from $15.15\,\mathrm{m^2\,g^{-1}}$ to $639.41\,\mathrm{m^2\,g^{-1}}$, and the GAB based SSA values range from $15.93\,\mathrm{m^2\,g^{-1}}$ to $915.32\,\mathrm{m^2\,g^{-1}}$. The commonly used BET equation gives the lower SSA values compared with GAB. Specific Surface Area values calculated from GAB based exceed the BET based values by about $21.6\,\%$ to $233.3\,\%$over the entire measured range. The results from GAB model is considered more accurate because the water activity range in GAB model is from 0.05 to 0.95 while it is 0.05 to 0.35 in BET model. The relation between the SSA values from BET and GAB models can be best fit by a linear model, which can be expressed by the following equation (R^2=0.95):

$$SSA_{GAB} = 1.24 \times SSA_{BET} + 17.12 \tag{4.3}$$

with

$$R^2 = 0.95 \tag{4.4}$$

4.3 Water Vapor Sorption Isotherms

The water vapor sorption isotherm of a soil describes the relationship between the relative humidity and water content. Figure 4.27 shows water vapor sorption isotherms of four clay minerals and three Alabama benchmarks soils obtained along both absorption and desorption

Table 4.2: Specific Surface Area of Studied Media from both BET and GAB models, SE indicates the Standard Error(n=2).

Type	Media	BET-SSA (m^2/g) $\pm$ SE (m^2/g)	GAB-SSA (m^2/g) $\pm$ SE (m^2/g)
Clay Minerals	KGa-1b	15.15 ± 1.12	15.94 ± 0.96
	KGa-2	21.19 ± 0.05	22.86 ± 0.02
	ISCz-1	97.53 ± 24.84	148.98 ± 11.13
	SHCa-1	127.81 ± 23.30	190.10 ± 4.12
	SWy-3	149.90 ± 13.24	192.24 ± 13.46
	SYn-1	178.76 ± 39.49	200.93 ± 44.22
	STx-1b	220.05 ± 59.12	266.61 ± 65.75
	PFI-1	314.30 ± 94.25	384.93 ± 111.98
	SAz-1	639.41 ± 219.06	915.31 ± 247.37
Benchmark Soils	Orangeburg	26.76 ± 0.91	32.85 ± 2.89
	Dothan	26.74 ± 0.43	46.25 ± 10.28
	Cecil	23.05 ± 0.49	45.08 ± 14.77

paths. Overall the sorption isotherms clearly show the positive relationship between relative humidity and soil water content, in which the a_w ranges from 0.03 to 0.95. The hysteresis phenomenon between the absorption and desorption isotherm is evident for all test media. The adsorption isotherm has a lower water content than the desorption isotherm at a given relative humidity.

The water sorption isotherms measured in this study are all sigmoidal-shaped isotherms, which can be divided into three stages. The first stage of the sorption isotherm is convex to the RH axis, the water molecules sorb onto the available sorption sites rapidly until a monolayer is formed, which is the result of Van der Waals forces on water molecules. After that, there is a stable and progressively increase of water content in the second stage. This is because the surface of the test media has already been saturated. It is characterized by the adsorption of water molecules on the first layer resulting in the creation of more layers. The isotherm in this zone can be represented graphically as growing linearly. There is abruptly increase in water content in the third stage where it is possible to find water in the liquid state in the soil capillaries. Assuming that in the interface from stage 2 to stage 3 the adsorbed water covers the soil particles homogeneously, the water molecule layer is thick enough to form liquid water in the pores

between soil particles by capillary condensation. Thus, micro capillary water starts to form a continuous phase.

The water vapor sorption isotherms were then used to estimate the monolayer corresponding relative humidity along with the monolayer water content of the test media. One of the benchmark soils, which was Orangeburg soil has a relatively low monolayer water content and it was not able to find a monolayer corresponding relative humidity on the water vapor sorption isotherm. The monolayer corresponding relative humidity values can be found in Table 4.3.

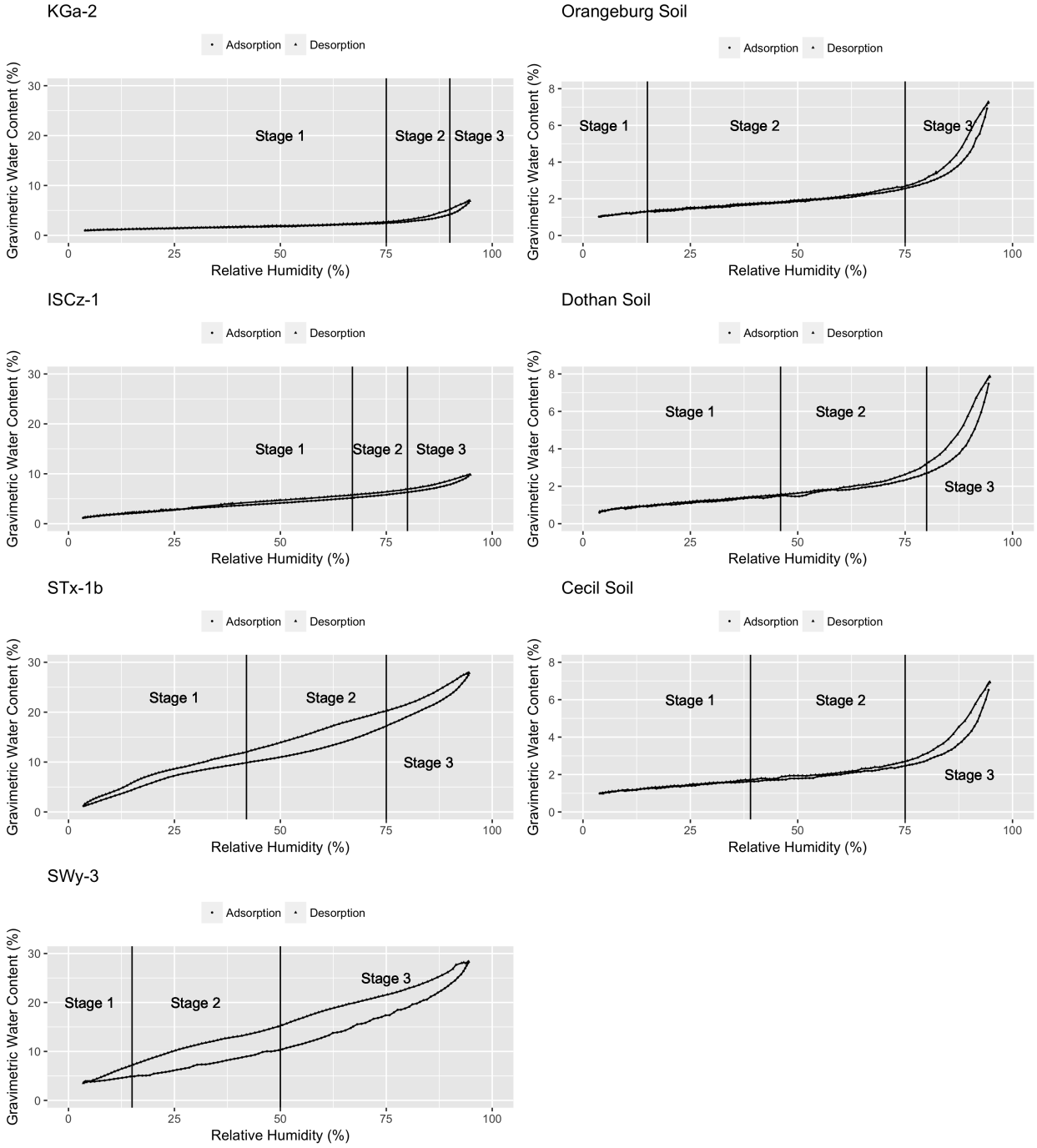

Figure 4.27: Water vapor sorption isotherms of test media. There are three stages in each isotherm, the first stage is the formation of monolayer, there is a stable increasing of water content in the second stage and rapid increasing of water content in the third stage.

4.4 Effect of Relative Humidity on 2,4-D Volatilization

Schneider and Goss (2012) studied the volatilization of pesticides from soils under dry conditions. Results showed the volatilization rate of pesticides could be significantly influenced by sorption to the hydrated mineral surface. This experiment started with very dry conditions, the volatilization rate of pesticides increases up to 8 times with an increasing relative humidity from $60\,\%$ to $85\,\%$. There was an additional strong increase of volatilization rate caused by a simulated rain event, which due to the elimination of all sorption sites associated to soil mineral surface. This study suggested that the surface area of mineral was the soil property that governs the volatilization of pesticides under dry conditions, and soil organic matter content was the controlling variable under wet conditions. Schneider and Goss (2012) also demonstrated that relative humidity effects on pesticide volatilization could be interpreted via the mechanism of sorption to the mineral surface under dry conditions.

In this study, I conducted volatilization experiments with six test media, which were Kaolinite (KGa-2), Na-rich Montmorillonite (SWy-3), Ca-rich Montmorillonite (STx-1b), Illite-smectite (ISCz-1), Cecil soil and Dothan soil. All the test media were exposed to different relative humidity levels, in which two of them were higher than m_0-RH and the other two were lower (Table 4.3).

Figure 4.28 shows the results of all the six test media under the relative humidity below and above monolayer water content related relative humidity. There were three replicates for each

Table 4.3: 2,4-D Volatilization Experiment Conditions: Two Above m_0-RH and Two Below m_0-RH.

Media	m_0 (%)	m_0-RH (%)	RH_1 (%)	RH_2 (%)	RH_3 (%)	RH_4 (%)
KGa-2	3.03	88	15	35	90	95
ISCz-1	5.19	67	15	60	75	90
SWy-3	5.39	15	5	10	35	65
STx-1b	7.37	42	15	25	60	80
Dothan	1.56	46	15	25	60	80
Cecil	1.65	39	15	25	60	80

relative humidity regime. The vertical line in the plots is the relative humidity corresponds to the monolayer water content of the test media (Table 4.3).

The volatilization rate of 2,4-D amine is relatively high, which ranges from $50\,\%$ to $80\,\%$. According to Figure 4.28, relative humidity is not a key factor that influences 2,4-D amine volatilization within $24\,\mathrm{h}$. The volatilization rate of 2,4-D amine on the surface of Kaolinite is driven by monolayer water content. The volatilization rate of 2,4-D amine in Kaolinite (KGa-2) at 35% is significantly lower than other relative humidity levels. The volatilization rate is significantly higher when the relative humidity is higher than monolayer water content corresponding relative humidity (p=0.06). The standard errors of the mean of the volatilization rate range from $0.25\,\%$ to $11.49\,\%$, the mean of the standard error is 2.76.

Compared with the study of Martina Schneider and Goss (2013), there is not a strong increase of volatilization rate when the relative humidity is higher than m_0-RH, the reason could be we used different herbicides, the properties of the herbicide might be a factor that influence the volatilization rate. Other than that, the overall experiment setting is not the same as well.

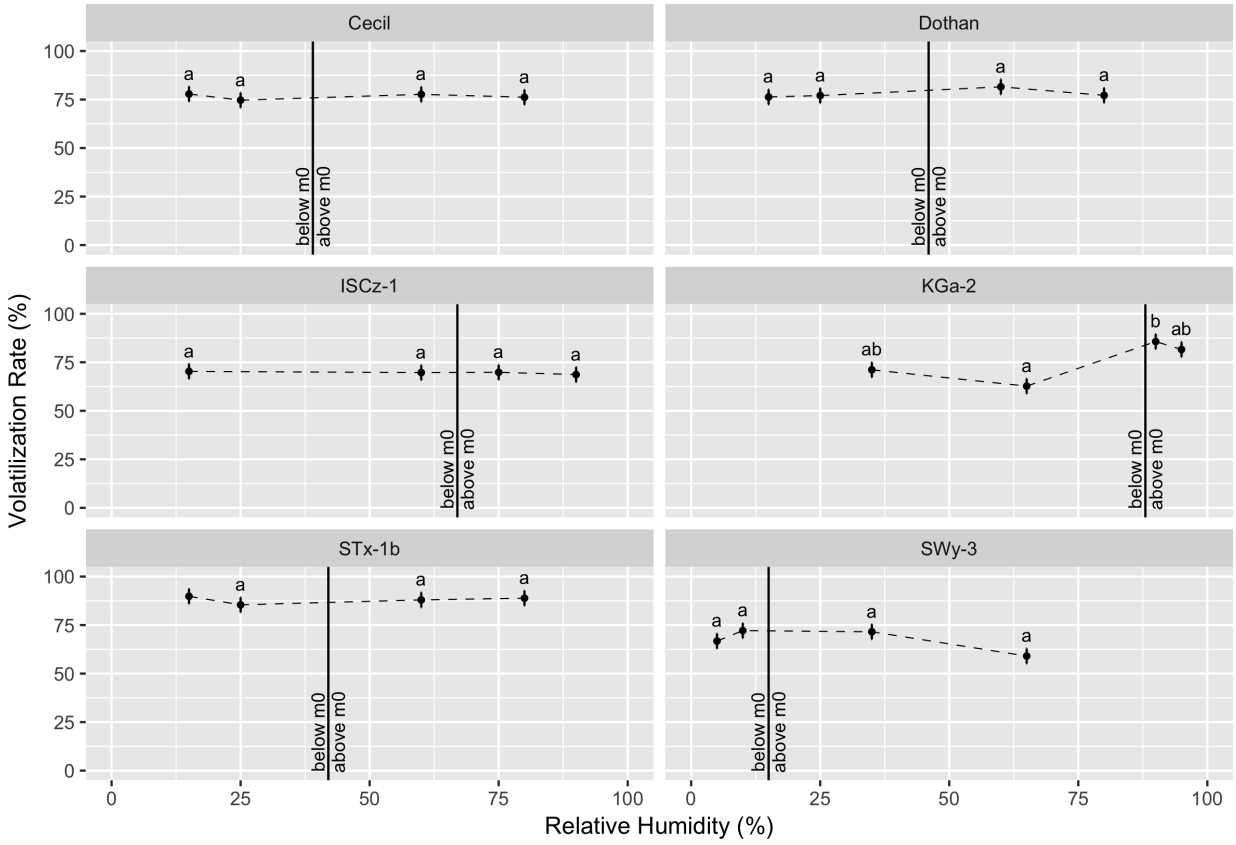

Figure 4.28: 2,4-D Volatilization Rate of Different Test Media in Variable Relative Humidity Levels, error bars are indicated in each RH level (n=3).

4.5 Daily Temperature and Relative Humidity Simulation

Figure 4.29 shows the air temperature and soil surface temperature from April 9th to 20th, 2017, which is the typical 2,4-D application season. The soil surface temperature ranges from $0\,^{\circ}\mathrm{C}$ to $73\,^{\circ}\mathrm{C}$, the air temperature were damped ranging from $5\,^{\circ}\mathrm{C}$ to $28\,^{\circ}\mathrm{C}$. Soil has a higher heat capacity and that is why the soil surface temperature has a higher range. The soil surface temperature exceeds the air temperature by 12.9% in average, and up to 163.4% at noon. At the beginning of April 10th, the soil temperature is higher than the soil surface temperature. This is because the higher heat capacity of the ground results in a later temperature decrease than the air. Later on the air temperature starts exceeding the soil surface temperature at around 3:00am as the release of latent heat from the ground. The soil surface temperature starts increasing and exceeds the air temperature as the rising of the sun. The soil surface temperature exceeds the air temperature up to 163.4% at 2:00pm. The solar radiation value has a positive relationship with both air temperature and soil surface temperature (Figure 4.30).

Figure 4.31 shows the relative humidity in the air and simulated relative humidity at soil surface from April 9th to 20th, 2017. The relative humidity value has a negative relationship with temperature. The relative humidity is decreasing as the increasing of the temperature. The air relative humidity for the selected days ranges from 24 to 100%, while the relative humidity at soil surface from 36 to 87%. The relative humidity in the air exceeds the soil surface relative humidity by 12.9% in average. The relative humidity at the soil surface is lower than the air relative humidity at night, and sometimes relative humidity in the air can reach 100%. The reason could be that the relative humidity at the soil surface can be balanced by the soil radiation damping. At noon time, the air relative humidity is lower than relative humidity at the soil surface, this is because The relative humidity in the air is lower than the soil surface relative humidity at midnight. There is a lag of the peak relative humidity value on the soil surface compared with in the air. This is because the relative humidity at the soil surface can be balanced by the ground.

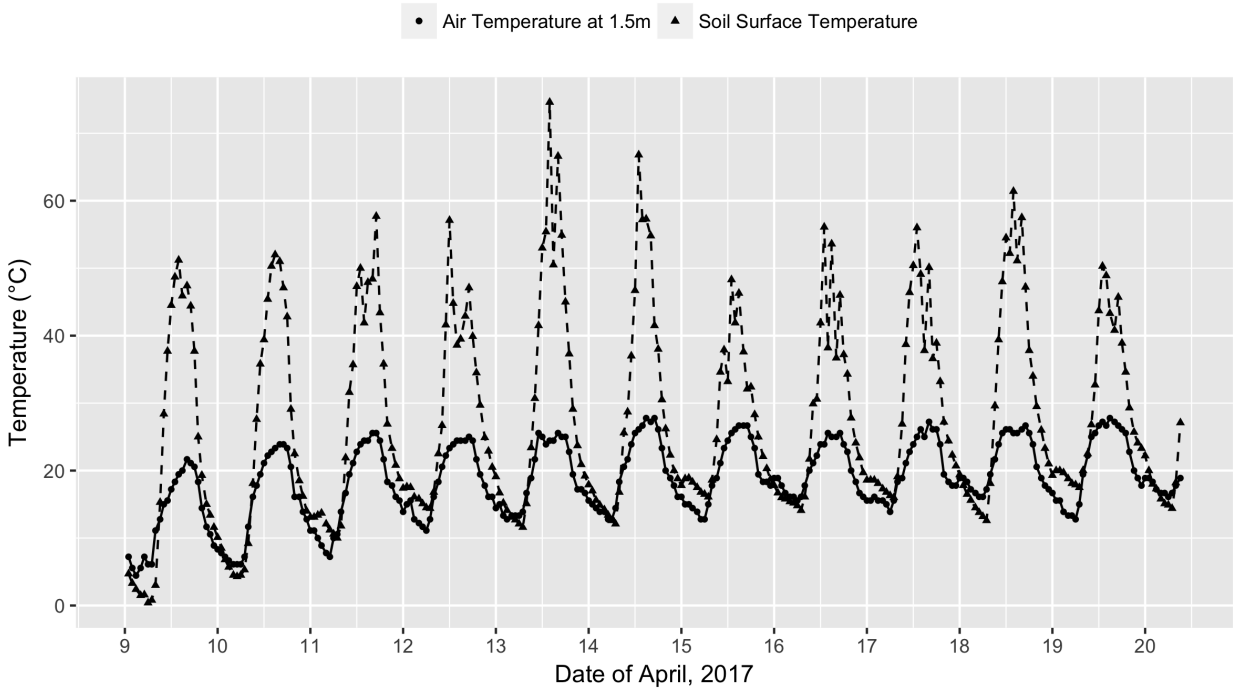

Figure 4.29: The Air Temperature and Soil Surface Temperature from April 9th to 20th, 2017.

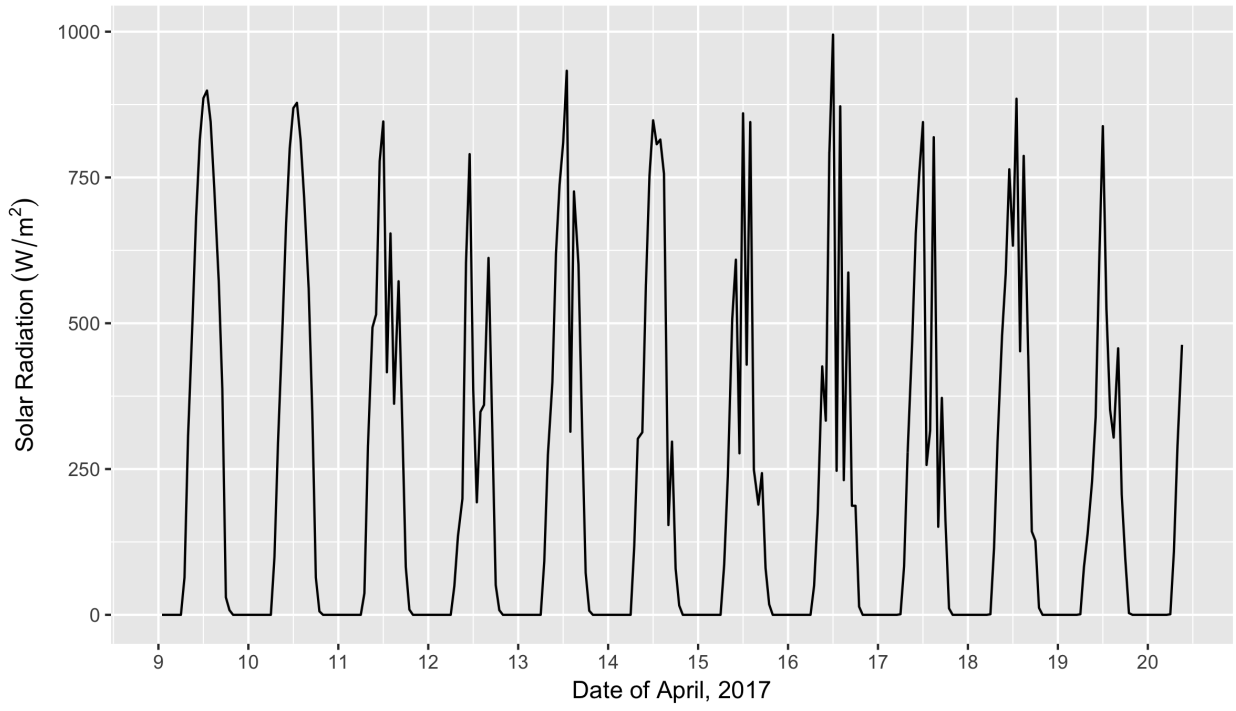

Figure 4.30: The Solar Radiation Values from April 9th to 20th, 2017.

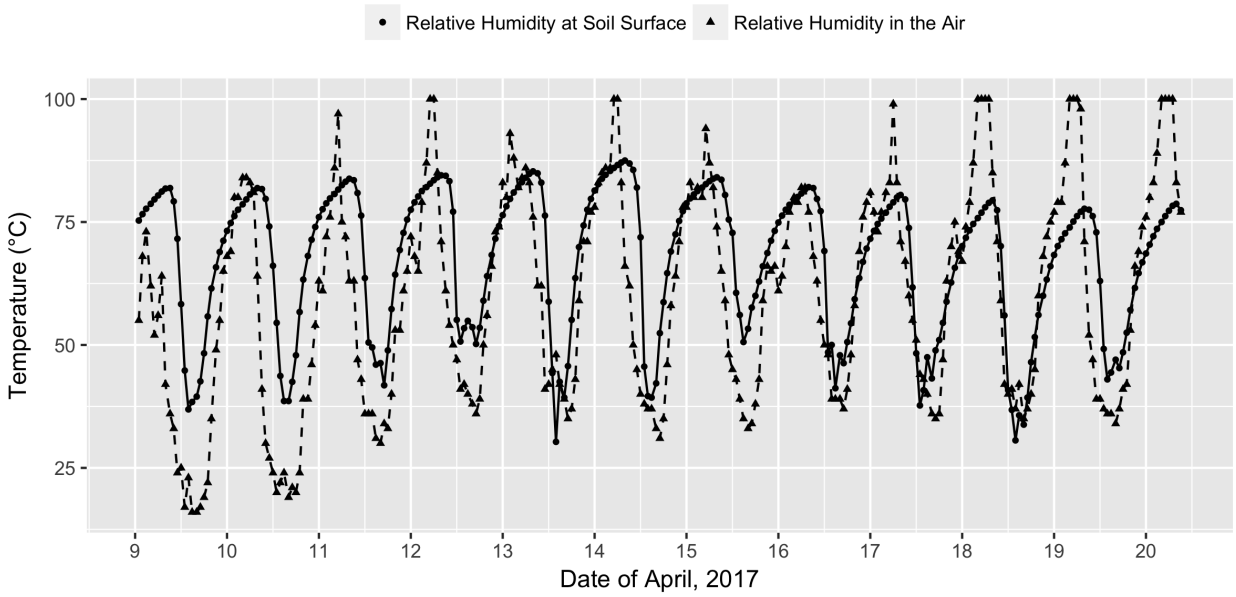

Figure 4.31: The Air Relative Humidity and Simulated Relative Humidity at Soil Surface from April 9th to 20th, 2017.

Chapter 5

Conclusions

The monolayer water content and specific surface area (SSA) are important properties for clay minerals and soils. Compared with the traditional determination method, the method mentioned in this study is more efficient and accurate. The two mathematical functions: BET and GAB models were used to calculate the monolayer water content and SSA. The commonly used BET equation resulted in lower monolayer water content and SSA values compared with GAB. The results from the GAB model is considered more accurate because the water activity range in GAB model is from 0.05 to 0.95 while it is 0.05 to 0.35 in BET model.

Measured water vapor sorption isotherms clearly illustrate the positive relationship between the relative humidity and water content. The hysteresis phenomenon between the absorption and desorption isotherm is evident for all test media. The adsorption isotherm has a lower water content than the desorption isotherm at a given relative humidity. The water vapor sorption isotherms of all the test media were developed by Vapor Sorption Analyzer (VSA) with relatively high resolution and reasonable time compared with the traditional dynamic vapor sorption method.

The very common used herbicide 2,4-D amine has a relative high dissipation rate, which ranged from $50\,\%$ to $80\,\%$. The dissipation rate of 2,4-D in different relative humidity levels was determined. The dissipation rate of 2,4-D amine in Kaolinite (KGa-2) at 35% is significantly lower than other relative humidity levels. Other than that, relative humidity was found to have a negligible effect on 2,4-D dissipation rate. The standard errors of the mean (n=3) of the volatilization rate range from $0.25\,\%$ to $11.49\,\%$, the mean of the standard error is 2.76. The VSA was used to simulate the real environment situation, which is more convenient and reproducible. This method can be used to evaluate more herbicides.

The relative humidity value has a negative relationship with temperature. The relative humidity is decreasing as the increasing of the temperature in a daily cycle. The temperature and relative humidity at soil surface is different from air. The soil surface temperature exceeds the air temperature by 12.9% in average, and up to 163.4% at noon. The relative humidity in the air exceeds the soil surface relative humidity by 12.9% in average. The relative humidity at the soil surface is lower than relative humidity in the air at night, and sometimes relative humidity in the air can reach 100%.

Many soil chemical and physical properties are effected by the ambient temperature and relative humidity. The diurnal temperature and relative humidity variations affect the herbicide volatilization process. Temperature and relative humidity variations can influence some fate and transport parameters producing significant diurnal cycles. These variations could have a significant effect on the volatilization process. More 2,4-D volatilization experiments will be done to evaluate the dissipation of 2,4-D in different diurnal temperature and relative humidity cycles.

Bibliography

2,4-dichlorophenoxyacetic acid (2,4-d) and its salts and esters, July 2011. URL https://oehha.ca.gov/media/downloads/crnr/10121124dcic.pdf. 08-23-2017.

I. D. Akin and W. J. Likos. Specific surface area of clay using water vapor and EGME sorption methods. Geotech. Test. J., 37(6), 2014.

Anon. Chemical Watch Factsheet 2,4-D, 2015.

E. Arthur, M. Tuller, P. Moldrup, and L. W. De Jonge. Evaluation of theoretical and empirical water vapor sorption isotherm models for soils. Water Resour. Res., 52(1):190–205, 2016.

J. M. Bingham, D. C. Golden, S. W. Buol, S. B. Weed, and L. H. Bowen. Iron oxide mineralogy of well-drained Ultosols and Osisals: II. Influence on color, surface area and Phosphate Retention. Soil Sci. Soc. Am. J., 42(January 1978):825–830., 1978.

S. Brunauer, P. H. Emmett, and E. Teller. Adsorption of Gases in Multimolecular Layers. J. Am. Chem. Soc., 60(1):309–319, 1938.

S. Brunauer, L. S. Deming, W. E. Deming, and E. Teller. On a Theory of the van der Waals Adsorption of Gases. J. Am. Chem. Soc., 62(7):1723–1732, 1940.

G. N. Callum Hill, Andrew Norton. The water vapor sorption behavior of natural fibers. Wiley InterScience, February 2009.

G. S. Campbell, D. M. Smith, and B. L. Teare. Application of a Dew Point Method to Obtain the Soil Water Characteristic. Vasa, 10(February):71–77, 2008.

Y. S. Catherine N. Mulligan, Masaharu Fukue. Sediments Contamination and Sustainable Remediation. Science, Dec 2009.

D. Charles. New gmos get a regulatory green light, with a hint of yellow, Oct 2014. URL http://www.npr.org/sections/thesalt/2014/10/15/356416365/new-gmos-get-a-regulatory-green-light-with-a-hint-of-yellow. 08-17-2017.

H. T. J. Charles JM. Developmental toxicity studies in rats and rabbits on 2,4-dichlorophenoxyacetic acid and its forms. developmental toxicity studies in rats and rabbits on 2,4-dichlorophenoxyacetic acid and its forms. Toxicol Science, March 2001.

J. S. B. Chipera D. L., J. S. B. Chipera D. L., S. J. Chipera, and D. L. Bish. Baseline Studies of the Clay Minerals Society Source Clays: Powder X-Ray Diffraction Analyses. Clays Clay Miner., 49(5):398, 2001.

K. A. Connors. Chemical kinetics: the study of reaction rates in solution. John Wiley & Sons, 1990.

P. M. Costanzo. Baseline studies of the clay minerals society source clays: Introduction. Clays and Clay Minerals, 49(5):372–373, 2001.

M. Cowbrough. Herbicide injury scenarios in soybeans and edible beans 2011, July 2011. URL http://fieldcropnews.com/2011/07/herbicide-injury-scenarios-in-soybeans-and-edible-beans-2011/.

M. Data. Kaolinite, 2001.

J. W. Deardorff. Efficient prediction of ground surface temperature and moisture, with inclusion of a layer of vegetation. J. Geophys. Res., 83(7):1889, 1978.

W. A. H. Deer. An Introduction to the Rock-Forming Minerals. Mineralogical Society of Great Britain and Ireland, 2013. ISBN 978-0-903056-43-4.

T. Delvalle. Amines or esters; which should you use. PennState Extension, 2017.

A. G. Dexter. Herbicide spray drift. North Dakota State University Extension Service, 657(August 1993):1–11, 1995.

A. U. Dogan, M. Dogan, M. Onal, Y. Sarikaya, A. Aburub, and D. E. Wurster. Baseline studies of the Clay Minerals Society source clays: Specific surface area by the BET method. Clays Clay Miner., 54(1):62–66, 2006.

M. Dogan, A. Umran Dogan, F. Irem Yesilyurt, D. Alaygut, I. Buckner, and D. E. Wurster. Baseline studies of the Clay Minerals Society Special Clays: Specific suerface area by the Brunauer Emmett Teller (BET) method. Clays Clay Miner., 55(5):534–541, 2007.

D. B. Donald, N. P. Gurprasad, L. Quinnett-Abbott, and K. Cash. Diffuse geographic distribution of herbicides in northern prairie wetlands. Environ. Toxicol. Chem., 20(2):273–279, 2001.

M. D. Douglas J. Parker, editor. Meterotology of Tropical West Africa. World Meterotology Organization, 2017.

EPA. 2,4-d choline salt, May 2015.

C. Feller. N2-bet specific surface areas of some low activity clay soils and their relationships with secondary constituents and organic matter contents. Soil Science, 153(4):293–299, April 1992.

Y. Fujita. The Determination Method of Surface Area by the BET Method. Shinku, 6(5):169–176, 1963.

J. D. Gaynor, C. S. Tan, C. F. Drury, T. W. Welacky, H. Y. F. Ng, and W. D. Reynolds. Runoff and drainage losses of atrazine, metribuzin, and metolachlor in three water management systems. J. Environ. Qual., 31(1):300–308, 2002.

P. Gentine, J. Polcher, and D. Entekhabi. Harmonic propagation of variability in surface energy balance within a coupled soil-vegetation-atmosphere system. Water Resour. Res., 47(5), 2011.

T. Gish. Relevance of pesticide volatilization, August 2017. URL https://www.ars.usda.gov/northeast-area/

beltsville-md/beltsville-agricultural-research-center/hydrology-and-remote-sensing-laboratory/docs/pesticide-volatilization/.

T. J. Gish, J. H. Prueger, W. P. Kustas, C. S. T. Daughtry, L. G. McKee, A. Russ, and J. L. Hatfield. Soil moisture and metolachlor volatilization observations over three years. J. Environ. Qual., 38 (5):1785–1795, 2009.

T. J. Gish, J. H. Prueger, C. S. Daughtry, W. P. Kustas, L. G. McKee, A. L. Russ, and J. L. Hatfield. Comparison of Field-scale Herbicide Runoff and Volatilization Losses: An Eight-Year Field Investigation. J. Environ. Qual., 40(5):1432, 2011.

K.-U. Goss and M. Madliger. Estimation of water transport based on in situ measurements of relative humidity and temperature in a dry Tanzanian soil. Water Resour. Res., 43(5):n/a–n/a, 2007.

A. Grube and Donaldson. Pesticides Industry Sales and Usage: 2006 and 2007 Market Estimates. U.S. Environ. Prot. Agency, page 41, 2011.

S. Guggenheim and K. A. F. van Groos. Baseline studies of the clay minerals society source clays: thermal analysis. Clays, 49(5):433–443, 2001.

B. Hammer, David. McLeese. Benchmark soils: Status and questions, September 2017.

S. Hillier. Clay and minerals, August 2017. URL http://www.claysandminerals.com/minerals/clayminerals.

P. Industrial and D. S. Pino. Evaluation of Wood Sorption Models for High Temperatures. Maderas. Cienc. y Tecnol., 7(2):143–158, 2005.

C. Kiranoudis, Z. Maroulis, E. Tsami, and D. Marinoskouris. Equilibrium Moisture-Content and Heat of Desorption of Some Vegetables. J. Food Eng., 20(1):55–74, 1992.

E.-C. Leong, S. Tripathy, and H. Rahardjo. Total suction measurement of unsaturated soils with a device using the chilled-mirror dew-point technique. Géotechnique, 53(2):173–182, 2003.

G. F. S. Louis B. Rockland. Water Activity: Influences on Food Quality. 978-0-12-591350-8. Louis B. Rockland, George F. Stewart, 1981.

N. Lu and M. Khorshidi. Mechanisms for Soil-Water Retention and Hysteresis at High Suction Range. J. Geotech. Geoenvironmental Eng., 141(8):04015032, 2015.

J. Madejova and P. Komadel. Base Line Studies of the Clay Minerals Society Source Clays: Infrared Methods. Clays and Clay Minerals, 49(5):410–432, 2001.

S. Mali, L. S. Sakanaka, F. Yamashita, and M. V. E. Grossmann. Water sorption and mechanical properties of cassava starch films and their relation to plasticizing effect. Carbohydr. Polym., 60 (3):283–289, 2005.

F. V. Marco Bittelli. Coupling of heat, water vapor, and liquid water fluxes to compute evaporation in bare soils. Journal of Hydrology, pages 191–205, August 2008.

G. S. C. Marco Bittelli and F. Tomei. Soil Physics with Python. Marco Bittelli, Gaylon S. Campbell and Fausto Tomei, Great Clarendon Street, Oxford, United Kindom, 1st edition, July 2015.

Z. B. Maroulis, E. Tsami, D. Marinos-Kouris, and G. D. Saravacos. Application of the GAB model to the moisture sorption isotherms for dried fruits. J. Food Eng., 7(1):63–78, 1988.

S. E. Martina Schneider and K.-U. Goss. Volatilization of pesticides from the bare soil surface: Evaluation of the humidity eff ect. Journal of Environmental Quality, pages 844–851, April 2013.

M. Mathlouthi. Water content, water activity, water structure and the stability of foodstuffs. Food Control, 12(7):409–417, 2001.

P. J. Mccall, S. A. Vrona, and S. S. Kelley. Fate of Uniformly Carbon-14 Ring Labeled 2,4,5-Trichlorophenoxyacetic Acid and 2,4-Dic hlorop henoxyacet ic Acid. J. Agric. Food Chem, 29: 100–107, 1981.

A. R. Mermut and G. Lagaly. Baseline studies of the clay minerals society source clays: Layer-charge determination and characteristics of those minerals containing 2:1 layers. Clays and Clay Minerals, 49(5):393–397, 2001.

I. Meter Environment. Hyprop overview, 2015. URL https://www.decagon.com/en/soils/benchtop-instruments/hyprop/. Sep-30-2017.

I. Meter Environment. Aqualab vapor sorption analyzer, 2017. URL http://www.aqualab.com/products/moisture-analysis-meters-2/aqualab-vapor-sorption-analyzer/. 2-28-2017.

G. V. Middleton. Encyclopedia of sediments and sedimentary rocks, 2003.

W. Moll. The origin and development of the source clays program. Clays and Clay Minerals, Oct 2002.

W. F. J. Moll. Baseline studies of the clay mineral society source clays: geological origin. Clays Clay Miner., 49(5):374–380, 2001.

Mollier. Mollier diagram, September 2017. URL http://www.alpicair.ee/et/tehniline-info-tugi/nouanded/mollier-diagram/. Sep-19-2017.

A. Muza. Growth regulator herbicides and grapes don't mix, Oct 2015. URL https://psuwineandgrapes.wordpress.com/2015/10/16/growth-regulator-herbicides-and-grapes-dont-mix/.

J. F. Nichelle Harriott. Environmentalists, farmers challenge usda's call for the deregulation of crops with genetically engineered tolerance to the highly toxic herbicide 2,4-d, January 2014. Jan 03, 2014.

NRCS. Cecil series, February 2007. URL https://soilseries.sc.egov.usda.gov/OSD_Docs/C/CECIL.html. Sep-17-2017.

NRCS. Orangeburg series, Dec 2014. URL https://soilseries.sc.egov.usda.gov/OSD_Docs/O/ORANGEBURG.html. Sep-17-2017.

NRCS. Cecil soil profile, September 2017a. URL https://www.nrcs.usda.gov/wps/portal/nrcs/detail/soils/survey/office/ssr7/profile/?cid=nrcs142p2_047954. Sep-17-2017.

NRCS. Dothan series, September 2017b. URL https://soilseries.sc.egov.usda.gov/OSD_Docs/D/DOTHAN.html. Sep-17-2017.

NRCS. Dothan soil profile, September 2017c. URL https://www.nrcs.usda.gov/wps/portal/nrcs/detail/soils/survey/office/ssr7/profile/?cid=nrcs142p2_047962. Sep-17-2017.

NRCS. Orangeburg soil profile, September 2017d. URL https://www.nrcs.usda.gov/wps/portal/nrcs/detail/soils/survey/office/ssr7/tr/?cid=nrcs142p2_048004. Sep-17-2017.

NRSC. Benchmark soils, August 2016. URL https://www.nrcs.usda.gov/wps/portal/nrcs/detail/soils/ref/?cid=nrcs142p2_054231. 08-23-2017.

I. E. Odom. Smectite clay Minerals: Properties and Uses. Philos. Trans. R. Soc. A Math. Phys. Eng. Sci., 311(1517):391–409, 1984. URL http://rsta.royalsocietypublishing.org/content/311/1517/391.short.

W. H. Organization. Environmental Health Criteria 84, Environmental Aspects - 2,4-Dichlorophenoxyacetic acid (2,4-D). International Programme on Chemical Safety, 1989.

A. Pollack. Dow corn, resistant to a weed killer, runs into opposition, April 2012.

F. Prothon and L. M. Ahrne. Application of the Guggenheim, Anderson and De Boer model to correlate water activity and moisture content during osmotic dehydration of apples. J. Food Eng., 61(3):467–470, 2004.

J. H. Prueger, J. L. Hatfield, and T. J. Sauer. Field-scale metolachlor volatilization flux estimates from broadcast and banded application methods in central Iowa. J. Environ. Qual., 28(1):75–81, 1999.

J. H. Prueger, T. J. Gish, L. L. McConnell, L. G. McKee, J. L. Hatfield, and W. P. Kustas. Solar radiation, relative humidity, and soil water effects on metalochlor volatilisation. Environ. Sci. Technol., 39:5219–5226, 2005.

S. S. Que Hee and R. G. Sutherland. Volatilization of various esters and salts of 2,4-D. Weed Sci., 22(4):313–318, 1974.

E. A. Rochette. Soil component interactions with 2,4-dichlorophenoxyacetic acid under supercritical fluid conditions. Environ. Sci. Technol., 30(4):1220–1226, 1996.

J. Rouquerol, D. Avnir, C. Fairbridge, D. Everett, J. Haynes, N. Pernicone, J. Ramsay, K. Sing, and K. Unger. Recommendations for the characterization of porous solids (technical report). Pure and Applied Chemistry, 66(8):1739–1758, 1994.

W. Schaer. The evaluation of gab constants from water vapor sorption data. Lebensmittel-Wissenschaft+Technologie, 18:225–229, 1988.

M. Schneider and K. U. Goss. Prediction of water retention curves for dry soils from an established pedotransfer function: Evaluation of the Webb model. Water Resour. Res., 48(6):1–5, 2012.

D. Schulze and U. Schwertmann. The influence of aluminium on iron oxides: X. properties of Al-substituted goethites. Clay Miner., 19(4):521–539, 1984.

U. Schwertmann. Properties of goethite and hematite in kaolinitic soils of southern and central brazil. Soil Science, 139(4):344–350, April 1985.

M. Sedighi, H. R. Thomas, P. J. Vardon, and B. D. P. Hepburn. Energy balance at the soil atmospheric interface. Environ. Geotech., pages 1–12, 2016.

A. W. Services. Awis weather service, May 2017. URL https://www.awis.com/index.html.

W. F. Spencer, W. J. Farmer, and M. M. Cliath. Pesticide volatilization, pages 1–47. Springer New York, New York, NY, 1973. ISBN 978-1-4613-9377-1.

A. W. Taylor and W. F. Spencer. Volatilization and Vapor Transport Processes. Soil Science Society of America, Soil Science Society of America, Madison, WI, 1990.

E. O. Timmermann. Multilayer sorption parameters: BET or GAB values? Colloids Surfaces A Physicochem. Eng. Asp., 220(1-3):235–260, 2003.

E. O. Timmermann, J. Chirife, and H. A. Iglesias. Water sorption isotherms of foods and foodstuffs: BET or GAB parameters? J. Food Eng., 48(1):19–31, 2001.

M. Tu, C. Hurd, and J. M. Randall. 2,4-D. Weed Control Methods Handb. Tools Tech. use Nat. areas, page 219, 2001.

P. University. Watch out for: Grapes, 2017. URL https://www.extension.purdue.edu/extmedia/ho/dw-10-w.pdf. 3-March-2017.

USEPA. 2,4-d red facts, June 2005. URL https://archive.epa.gov/pesticides/reregistration/web/html/24d_fs.html.

K. E. S. W. J. Rawls, D. L. Brakensiek. Estimation of soil water properties. American Society of Agricultural and Biological Engineers, 25(5):1316–1320, 1982.

D. Wager. Application for a derogation to use a highly hazardous pesticide, 2017. 08-23-2017.

C. Wang, J. Li, and H. Fang. Ordered water monolayer at room temperature. Rend. Lincei, 22 (SUPPL. 1), 2011.

R. D. Wauchope. The pesticide content of surface water draining from agricultural fields: A review. J. Environ. Qial., 7(4):459–472, 1978.

W. Wolf, W. E. L. Spiess, G. Jung, H. Weisser, H. Bizot, and R. B. Duckworth. The Water-Vapour Sorption Isotherms of Microcrystalline Cellulose (MCC) and of Purified Potato Starch. J. Food Eng., 3(1):51–73, 1984.

W. Wu. Baseline studies of the clay minerals society source clays: Colloid and surface phenomena. Clays and Clay Minerals, 49(5):446–452, 2001.

B. Youngman. Climate and earth's energy balance, August 2017. URL `https://serc.carleton.edu/earthlabs/weather_climate/lab_2.html`. Sep-19-2017.